5-2018

The postglacial sea level history of Ingøya, northern Norway

Sam Rickerich
srickeri@bates.edu

The postglacial sea level history of Ingøya, northern Norway

An Honors Thesis

Presented to

The Faculty of the Department of Geology

Bates College

In partial fulfillment of the requirements for the

Degree of Bachelor of Science

By

Sam F. Rickerich

Lewiston, Maine

April 16, 2018

Acknowledgements

Foremost, I would like to thank my advisor Mike Retelle for guiding me through both this study and through my years here as a student at Bates College. From inviting me to join the Ingøya team in 2016 and 2017, to setting the framework for a new and engaging area of study, and to providing valuable and necessary feedback throughout this project – I am very grateful for all that you have done. Thank you for providing me with numerous opportunities, fond memories, and the foundation of my understanding of climate science.

I would also like to extend my gratitude towards the mentorship of Lee Corbett and Paul Bierman of the University of Vermont. Lee, your guidance while working in the Cosmogenic Nuclide Laboratory was very much appreciated. To Bev Johnson and Phil Dostie, thank you for all your help throughout this process. Your willingness to work with me in the Environmental Geochemistry Laboratory was much appreciated. I would like to thank the whole Ingøya research team – Al Wanamaker, Michael Carroll, Julie Retelle, Ann and Thorleif Hansen, Dan Frost, and Maddie Mette – this work would not have been possible without you. Assistance of Pete Dawson in the RB Gilmore X-ray Fluorescence Laboratory, UMass Amherst Geoscience Department was much appreciated. Additionally, I would like to acknowledge Christine Murray and Louise Brogan for technical support with GIS and the imaging center. Thank you to the Bates Student Research Fund and to the National Science Foundation grant number 1417636 for providing funding. And lastly, I would like to acknowledge the whole Bates College Geology Department for their friendships and support over these years. Thank you.

Table of Contents

Table of Figures

Table of Tables

Abstract

Reconstructions of postglacial relative sea level history in formerly glaciated terrains reflect the interaction of glacioisostatic processes and ocean water volume changes, providing insight into regional ice sheet dynamics, crustal rheology, and meltwater fluxes. This study focuses on the relative sea level history of Ingøya, an island in the Finnmark region of northern Norway, which was located near the confluence of the Scandinavian Ice Sheet (SIS) and Barents Sea Ice Sheet (BSIS) during the Last Glacial Maximum. Previously undated raised beach sequences on Ingøya record isostatic and ocean water volume changes from the late glacial through the late Holocene. A combination of field, analytical and geochronogical approaches were utilized to constrain the timing and rate of relative sea level change. These include cosmogenic ^{10}Be surface exposure dating of boulders on raised shorelines, ^{14}C dating of the marine-lacustrine transition in an isolation basin, and ^{14}C dating of marine bivalves found in late Holocene raised beach deposits.

The uppermost raised marine shorelines on western Ingøya are a series of boulder beaches from 20 to 30 m asl that record the marine limit during deglaciation and initial isostatic emergence. The average ^{10}Be age of schist-quartzite boulders on the highest shoreline at 30 m asl is 14.8 ± 0.5 ka (average, 1 SD, n = 6, North East North American production rate). A second, lower cobble shoreline across the valley at 20 m asl has a similar age of 14.8 ± 0.3 ka (1 SD, n =2), indicating rapid isostatic uplift following deglaciation.

Sediment core radiocarbon ages on plant macrofossils from an isolation basin at 6 m asl further constrain the timing and extent of the mid-Holocene transgression and the 8.2 ka Storegga Tsunami. Maximum ages of 7590 ± 20 cal yr BP and 5318 ± 5 cal yr BP from woody macrofossils define the timing of inundation and isolation of the 6 m asl basin. The stratigraphic relationship between the coarse gravel unit below the 7590 ± 20 cal yr BP age suggests that this basin was inundated by the Storegga Tsunami. Projections of tsunami run-up of 3 – 5 m constrains relative sea level at 8.2 ka to range from 1 – 3 m above modern day levels.

On southern Ingøya, a flight of lower elevation gravelly raised beaches that contain abundant bivalve shells, mainly *Modiolus modiolus*, extends from near sea level to a prominent bench-like terrace at 9 m asl. A ^{14}C age of 6,450 ± 40 cal yr BP was obtained on a *Modiolus* shell from a trough directly below the highest terrace. The age of the upper terrace corresponds to similarly dated deposits in coastal northern Norway related to the mid-Holocene Tapes Transgression, during which sea level rise outpaced glacioisostatic rebound. The relative sea level history from Ingøya sheds light on the timing of deglaciation of the north Finnmark coast, the separation of BSIS and SIS, and the extent of the mid-Holocene transgression.

1. Introduction

Reconstructing postglacial sea level of a formerly glaciated region gives insight into ice sheet dynamics, crustal rheology, and rates of sea level change through time (Peltier, 1998). A comprehensive understanding of local sea level history is important when considering the current context of our changing climate. A better understanding of the past is important to anticipate the future. It is known that throughout the Quaternary, sea level has fluctuated alongside the Earth's climate in response to oscillatory glacial cycles (Lambeck and Chappell, 2001). Over the past 900 kyr, Earth's orbital parameters have driven glacial cycles with a 100 kyr period (Huybers and Wunsch, 2005). The relative elevation of sea level throughout these cycles is defined by glacial-eustasy on a global scale and by glacial-isostasy on a regional scale in glaciated areas (Andrews, 1974).

Low-stands in sea level reach -120 m on average during glacial maxima while during interglacial periods sea level obtains a relative high-stand (Andrews, 1974). Immediately after a glaciation, rapid isostatic uplift of the depressed lithosphere is the main control on regional sea level (Lambeck and Chappell, 2001). With time and further ice sheet retreat this effect is minimized and glacial-eustasy controls relative sea level (note, glacial-eustasy is used here synonymously with ocean-water-volume changes and the dynamic gravitational influence on sea level is recognized (Riva et al., 2010)). In Scandinavia, changes in relative sea level following the last glacial maximum (LGM) are controlled by deglaciation of the Scandinavian Ice Sheet (SIS) from ice maxima positions, the cool period of the Younger Dryas, and a transgressive period known as the Tapes Transgression in the mid Holocene (Wohlfarth et al., 2008). However, regional differences in deglaciation cause relative sea level history to vary throughout Scandinavia as synchronous shorelines appear at different elevations in different regions.

The purpose of this study is to better understand relative sea level history and its implications in northern Norway (71°N) since the last glacial maximum (LGM) through the reconstruction of postglacial isostatic emergence of the island of Ingøya, northern Finnmark (Figure 1). An understanding of the Scandinavian Ice Sheet (SIS) and the Barents Sea Ice Sheet (BSIS) history since the LGM is necessary in order understand the drivers of relative sea level change through time. The postglacial emergence history on this island in northern Norway is reconstructed using 1) surface exposure ages from cosmogenic ^{10}Be produced in situ in beach cobbles at marine limit, 2) radiocarbon dating of the marine-lacustrine sediment transition in an isolation basin, and 3) radiocarbon dating of marine bivalves found in raised shorelines. From this work, the isostatic uplift pattern of northern Norway can be refined and the retreat of the SIS can be further constrained in order to form a better picture of how ice sheets behave in a changing climate.

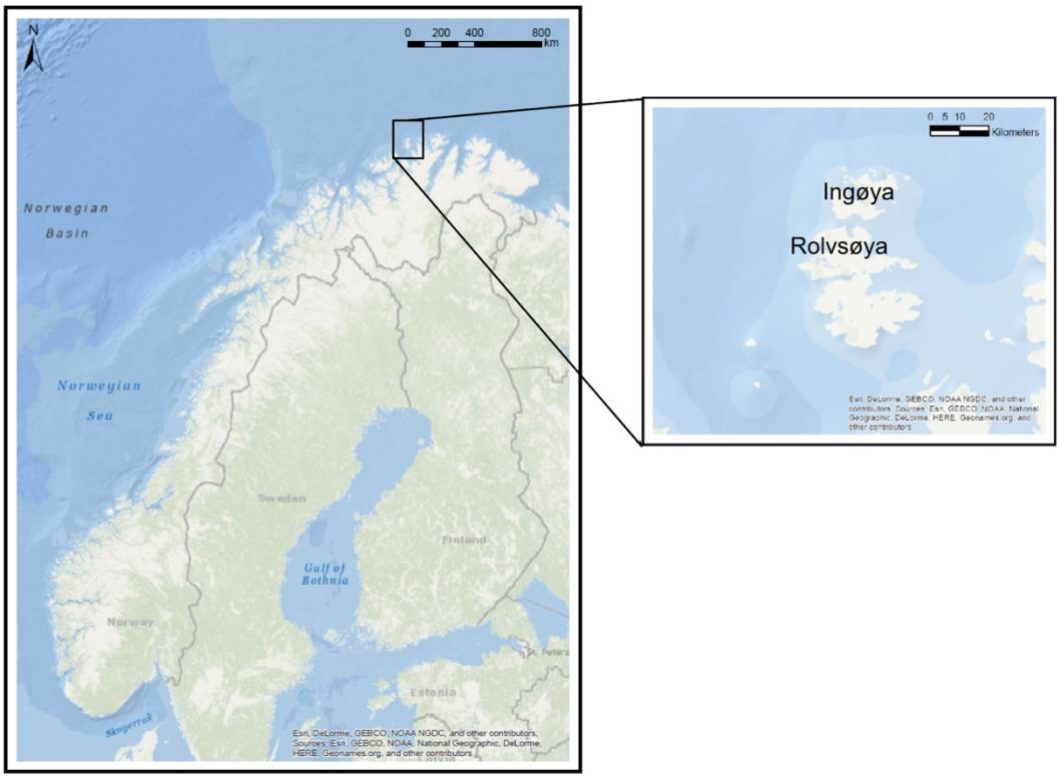

Figure 1. *The study location of Ingøya (north) and Rolvsøya (south).*

1.1. Glacial history

1.1.1 LGM in northern Eurasia

Over the past 120 ka northern Eurasia has experienced repeated glacial advances and interstadial periods characterized by the confluence and breakup of the Eurasian Ice Sheet (EurIS) complex (Hughes et al., 2016). This period starting at the end of Eemian (Marine Isotope Stage (MIS) 5e) can be broken up into the Early, Middle, and Late Weichselian glaciations (Mangerud et al., 2011). The Late Weichselian occurred between the between the Ålesund interstadial (36-34 ka) and MIS 1, during which the EurIS obtained its maximum extent (Figure 2) (Hughes et al., 2016; Mangerud et al., 2011; Mangerud et al., 1981).

Figure 2. *Hughes et al. (2016) reconstruction of the EurIS during the Late Weichselian. Dashed lines mark approximate boundaries of the BIIS, SIS, and SBKIS (termed BSIS in this work). Gray areas delineate submarine fans, and the red star is the study location.*

The EurIS complex was comprised of the Scandinavian Ice Sheet (SIS), the Barents Sea Ice Sheet (BSIS), and the British Isles Ice Sheet (BIIS) (Hughes et al., 2016; Larsen et al., 2016). The SIS was largely terrestrially based, save for ice maxima positions that extended onto the continental slope of the North Sea, Norwegian Sea, and Barents Sea (Larsen et al., 2016; Sejrup et al., 2009). To the north, the BSIS was a marine based ice sheet centered over the Barents Sea that converged with the SIS to the south during the LGM (Landvik et al., 1998; Winsborrow et al., 2010).

1.1.2. Late Weichselian reconstructions

Hughes et al.'s (2016) Late Weichselian reconstruction of the EurIS demonstrates that at ca. 21 ka, the ice sheet complex reached a maximum extent and volume at 5.5 Mkm^2 and 24 m sea level equivalent (Figure 3). This occurrence falls within the last global glacial maximum between ca. 23 – 21 ka (Clark et al., 2009).

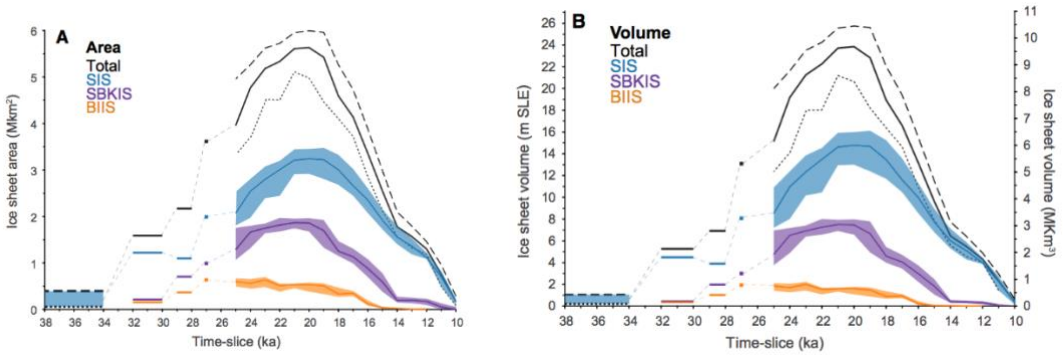

Figure 3. *Evolution of the EurIS's (A) ice sheet areas in Mkm^2 and (B) volumes in both m sea level equivalent and Mkm^3 from Hughes et al. (2016).*

The SIS was the largest ice sheet of the EurIS complex. The maximum extent of the SIS along its western border occurred between 29 – 25 ka while the eastern flank reached a maximum between 18 – 16 ka (Larsen et al., 2016). Along its western margin, the SIS terminated on the continental shelf break from the Norwegian Channel to the North Cape (Mangerud, 2004). Landforms indicative of both non-erosive cold-base and erosive warm-based ice exist throughout Scandinavia (Ottensen et al., 2007; Larsen et al., 2016). To the north, the SIS and BSIS primarily drained through the Bjørnøyrenna Ice Stream (Ottensen et al., 2008; Piasecka et al., 2016). Isobase maps derived from reconstructed relative sea level curves reflect the center of the ice mass in the north-central Barents Sea (Landvik et al., 1998). Modeling from isostatic uplift patterns results in a 2000 – 3000 m thick BSIS during the LGM (Landvik et al., 1998). The SIS and BSIS coalesced at 25 ka, nearly coincident with the maximum reconstruction of the BSIS (Hughes et al., 2016).

1.1.3. Deglaciation

Deglaciation of the EurIS can be divided into three intervals: 1) initial retreat, 2) the Younger Dryas readvance 3) and the final decay during the early Holocene (Mangerud, 2011). The deglaciation of the BSIS began along its western margin at 19 ka and was influenced by the rapid retreat of the Bjørnøyrenna Ice Stream (Winsborrow et al., 2010). Due to a lack of dates, the pattern of retreat is poorly constrained in the eastern Barents Sea between 17 – 15 ka, during which the southern Barents Sea became ice free (Hughes et al., 2016; Romundset et al., 2011). By the abrupt warming of the Bølling-Allerød period (14.6 ka), the outer coast of northern Norway became ice free and by 12 ka the SIS margin was split into lobe, valley, and fjord glaciers (Romundset et al., 2011; Hughes et al., 2016). Younger Dryas (12.7 – 11.5 ka) moraines can be mapped continuously throughout Scandinavia, indicative of a temporary readvance (Bergstrøm et al., 2005; Hughes et al., 2016; Mangerud et al., 2011). The disappearance of the SIS was likely complete by 9 ka (Hughes et al., 2016).

1.1.4. Northern Norway glacial landforms and ice retreat

Late Weichselian landforms in northern Norway include, but are not limited to, terminal moraines, raised shorelines, fjords, glacial lakes, and mega scale glacial lineations. North-south trending fjords guided ice flow and fed major ice streams on the Barents Sea floor (Ottensen et al., 2008). Onshore plateau icefields formed drumlins, eskers, and streamlined landforms that represent the same northern flow direction and warm based ice conditions (Sollid et al., 1973; Winsborrow et al., 2010).

The Egga submarine end moraines on the outer continental shelf mark the outermost extent of the SIS (Andersen, 1965). The northern coast of Scandinavia was ice free by 15 ka, as constrained by 14.3 ± 1.7 ka and 13.6 ± 1.4 ka ages on moraines from the Outer Porsanger sub-stage (Romundset et al., 2017). These ages are attributed to the cool period of the Older Dryas. The readvance of the SIS during the Younger Dryas deposited the Tromsø-Lyngen moraines that can be continuously mapped throughout northern Norway (Bergstrøm et al., 2005). These two major moraine systems, shown in Figure 4, mark the halt or readvance of the SIS during deglaciation.

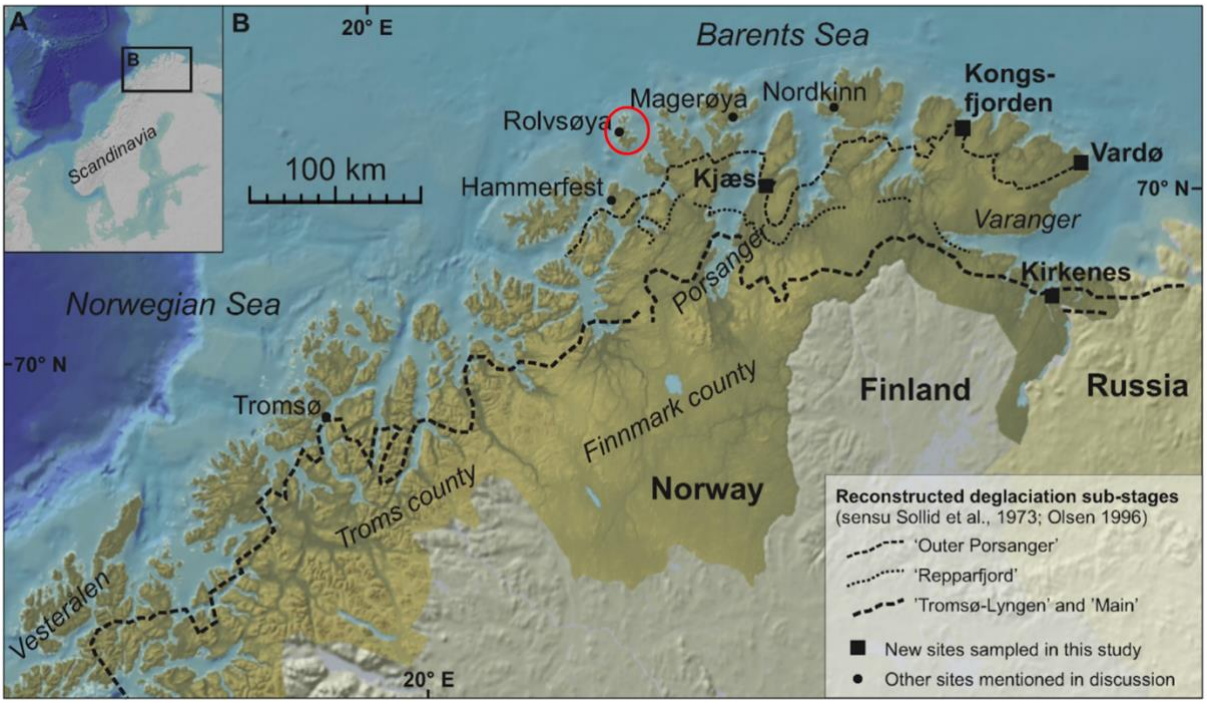

Figure 4. *Map of the two major moraines found throughout northern Norway. The Outer Porsanger and Tromsø-Lyngen correspond to the Older Dryas and Younger Dryas cool periods, respectively. From Romundset et al. (2017). The red circle encompasses the study location.*

1.2. Raised shorelines in northern Norway

Postglacial raised shorelines in northern Norway are classified as either late-glacial, post-glacial, or Tapes depending on their age and elevation (Evans et al., 2002). These raised

shorelines can be seen clearly along coastal regions due to the lack of forests in this arctic landscape (Sollid et al., 1973). Initial rates of postglacial uplift outpaced eustatic sea level rise, resulting in regression from marine limit and steep shoreline gradients (Sollid et al., 1973). This regression occurred through the Boreal period (9 – 7.5 ka), after which the Tapes Transgression – a eustatic rise in sea level, presumably from the melting of Antarctica and ice sheets in the Northern Hemisphere – defined the sea level history throughout the mid-Holocene (Marthinussen, 1962; Renssen et al., 2012; Sollid et al., 1973; Wohlfarth et al., 2008).

The earliest and uppermost marine limit shorelines are commonly marked by gravel or cobble beaches and abrasion marks from sea ice (Sollid et al., 1973). Marine limit elevations increase steadily to the south due to isostatic loading of the SIS, with the highest shoreline approximately 150 km inland from the Barents Sea at 145 m asl (Synge, 1969). The most prominent late-glacial shoreline along the northern Norwegian coast is the 10 ka Main shoreline. Andersen's (1965) Main shoreline isobase map is shown in Figure 5. Tromsø-Lyngen moraines are situated inside of the Main shoreline, and

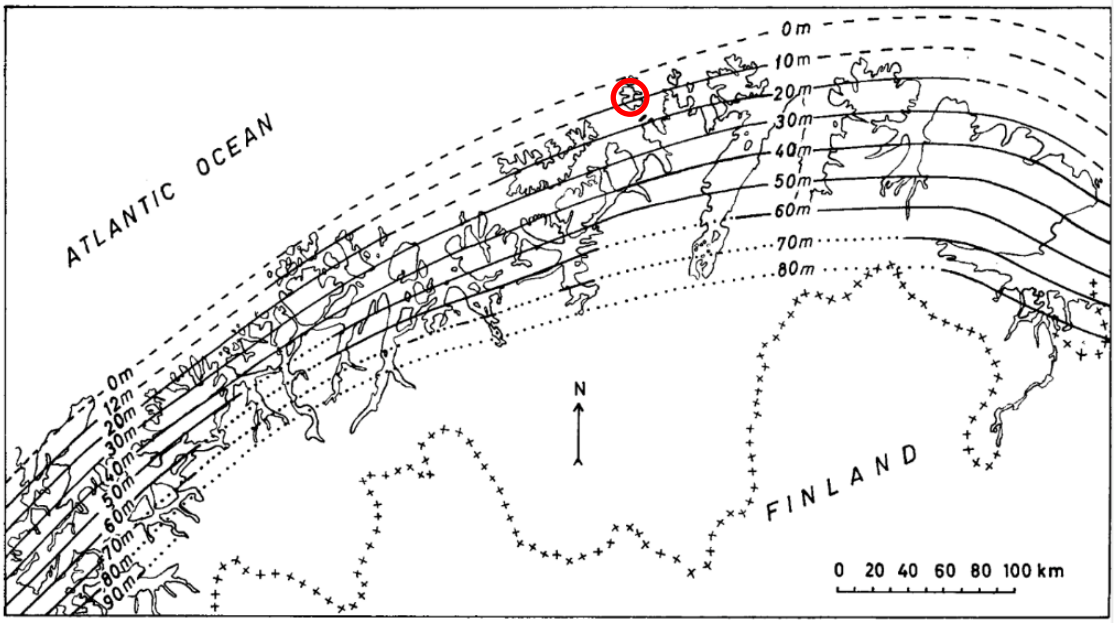

Figure 5. *10 ka isobase map, coincident with the Main shoreline. From Andersen (2016). The red circle shows the study location.*

outwash plains from these moraines grade into this shoreline, both of which indicate that they are of similar age (Andersen, 1965; Evans et al., 2002). The Main shoreline formed through beach processes in addition to frost shattering and erosion of sea ice bergs (Sollid et al., 1973).

Distinct postglacial shorelines formed after 10 ka exist throughout northern Norway (Marthinussen, 1962). Postglacial shorelines at slightly lower elevations than the Main shoreline relate to the Stordal Moraines (dated ca. 9 - 10 ka) (Andersen, 1965; Evans et al., 2002). No

driftwood or dateable materials have been found in these postglacial shorelines (Marthinussen, 1962). In some locations to the south of the study area, the regression reached 2 – 3 m below modern day sea level between 7.5 - 9.9 ka (Marthinussen, 1962). However, most postglacial shorelines are not easily observable since they were subsequently cross cut during the Tapes Transgression (Evans et al., 2002).

A global increase in ocean water volume during the Holocene Thermal Maximum initiated the Tapes Transgression, forming four distinct shorelines referred to as $T_{I,}$ T_{II}, T_{III}, and T_{IV} (Evans et al., 2002; Moossen et al., 2015). The increase in ocean water volume at this time may be attributed to the melting of the Laurentide, Greenland, and Antarctica. The 8.2 ka catastrophic drainage of the Laurentide's glacial lake Agassiz-Objibway through the Hudson Strait brought a massive (>10^{14} m^3) outflow of freshwater to the Labrador Sea and the North Atlantic (Barber et al., 1999). However, this would not be a large enough source to initiate the Tapes Transgression on its own. A large source of Holocene ocean water volume also came from the deglaciation of Antarctica. In comparison to the Northern Hemisphere ice sheets, the deglaciation of Antarctica was relatively delayed until 10 – 8 ka (Ingólfsson and Hjort, 1999). As a result, part of the increase in global ocean water volume from 8 – 7 ka, and most of it between 7 – 5 ka, is attributed to the deglaciation of Antarctica (Ingólfsson and Hjort, 1999).

Mid-Holocene shorelines are distinguishable throughout northern Scandinavia as well-developed, lower elevation raised beach ridges with a low shoreline gradient (Romundset et al., 2011; Snyder et al., 1996; Sollid et al., 1973). Evidence for a marine-transgression at this time in northern Norway was first discovered in eastern Finnmark through the occurrence of freshwater peat overlain by marine gravel and sand (Marthinussen, 1962). The peat is 8 m below the soil surface at an elevation of 24.5 m asl, and it is dated to 7.7 ka (Marthinussen, 1962). Radiocarbon dates from driftwood recovered from the Tapes shorelines range in age from 6.6 – 4.8 ka; specifically, T_I is dated to 6.6 – 6.5 ka, T_{III} to 5.7 – 5.5 ka, and T_{IV} to 4.8 – 4.5 ka (Marthinussen, 1962). Alternations between lacustrine, marine, and lacustrine sedimentation in several isolation basins suggests that the Tapes Transgression was a 3 ka period of stable sea level from 8 – 5 ka (Romundset et al., 2011). To the west on the Kola Peninsula in Russia, a transgressive shoreline dated at 6.2 – 6.6 ka is synchronous with the Tapes Transgression (Snyder et al., 1996). By 7 ka the Tapes Transgression had reached its maximum level, after which the remaining isostatic adjustments caused relative sea level to fall to today's current level (Wohlfarth et al., 2008).

1.3. Geochronological approaches for relative sea level reconstructions

The collection of sea level data through the Holocene began in the 1960's when the method of radiocarbon dating was applied to organic matter associated with raised shorelines (Mangerud, 1972). Radiocarbon ages on shells or bones or driftwood from raised shorelines yield maximum ages, due to their means of emplacement from an unknown source. A piece of

driftwood, for example, could be a result of a tree that died one hundred years prior to assuming a position on a shoreline. Additionally, the reworking of organic material will only stop after a shoreline is abandoned and sea level has fallen below it. Both of these factors must be considered when dating organic material from raised shorelines.

Radiocarbon dating requires several assumptions: 1) ^{14}C half-life is known, 2) ^{14}C activity at an organism's time of death is known, and 3) there is no exchange of carbon with the environment after death (Mangerud, 1972). Dateable organic material includes driftwood, bones, foraminifera, and shells. However, it is necessary to correct for radiocarbon ages because they are not equivalent to calendar years; ^{14}C concentrations vary through time due to the flux of cosmic rays in the upper atmosphere, which is ultimately controlled by the Earth's magnetic field (Reimer et al., 2013). In Norway, calibration of terrestrial ^{14}C ages is achieved through the correlation with tree rings dating back to 13.9 ka (Reimer et al., 2013).

Reservoirs of carbon, such as the atmosphere and ocean, have different residence times that alter the age derived from organic material and give apparent ages that are not representative of calendar years (Mangerud, 1972). In the ocean, organisms that produce carbonate shells do so in isotopic equilibrium with the body of water where they live. Since the apparent age of a body of water depends on circulation patterns, apparent ages range from 200 to 300 yrs to more than 2500 yrs depending on ocean circulation (Mangerud, 1972). As long as the apparent age of a body of water is known, accurate radiocarbon dating of raised shorelines is possible.

More recently, high precision reconstructions have been made possible through the dating of cosmogenic nuclides produced in situ in rocks on raised shorelines (Bierman et al., 2016). This technique is particularly useful in locations where organic material is not available for radiocarbon dating (Bierman et al., 2016). Cosmogenic nuclides are produced in both the upper atmosphere and in rocks due to interactions with cosmic rays (Ivy-Ochs and Kober, 2008). The wide array in half-life's of these nuclides makes them capable of dating landforms ranging from hundreds of years to millions of years old (Ivy-Ochs and Kober, 2008). Production rates of the radionuclides ^{10}Be, ^{14}C, ^{26}Al, and ^{36}Cl vary positive exponentially with altitude and latitude while they decrease exponentially with depth within a rock (Ivy-Ochs and Kober, 2008). In glaciated landscapes with warm-based erosive ice, cosmogenic radionuclide production begins once the landscape is exposed through either the retreat of an ice sheet or a fall in relative sea level (Bierman et al., 2016). Most of the cosmogenic nuclide ^{10}Be at the surface of rocks is produced by the spallation of ^{16}O in the lattice structure of quartz minerals, while at depth in a rock muon capture produces ^{10}Be at a lower rate (Ivy-Ochs and Kober, 2008).

If sufficient erosive conditions exist that remove surfaces that were exposed during prior ice free periods, surface exposure dating should not be affected by inherited ages from residual cosmogenic nuclides (Bierman et al., 2016). To remove all possible cosmogenic nuclides from a rock it is necessary to erode over 2 m from the rock surface (Ivy-Ochs and Kober, 2008). For simplicity, it is assumed that there are no preexisting cosmogenic nuclides upon the emplacement/exposure of a bedrock or boulder sample. Hence, it is sufficient to just account for surficial erosion rates and ongoing beach processes that each beach cobble is subjected to.

Similar to radiocarbon samples from raised shorelines, the abandonment of beach cobbles on raised shorelines as sea level falls marks a sharp decrease in erosive conditions and the possible reworking or overturning of cobbles. Since beach cobbles on raised shorelines contemporaneous with sea level experience higher rates of erosion, exposure ages give a minimum estimate for the formation of raised shorelines. At the very least, it is known that the cosmogenic production within beach cobbles starts at a constant, uninterrupted rate once a shoreline is no longer active.

1.4. Postglacial sea level reconstruction in Finnmark, Norway

On Rolvsøya, Sørøya, and the Nordkinn peninsula (Figure 6) three postglacial sea level curves (Figure 7) were constructed by Romundset et al. (2011) through the isolation basin method. The following is a brief summary of this work.

Basal ages from a sediment core from Rolvsøya mark the deglaciation of the outer coast of Finnmark at 14.6 ka. These ages were used to infer the timing of deglaciation as well as the near synchronous establishment of marine limit in this location, which was mapped at 45 m asl (Marthinussen, 1960). The relatively low elevation of marine limit was attributed to the isostatic uplift of the Barents Sea floor prior to deglaciation of the north coast of Finnmark.

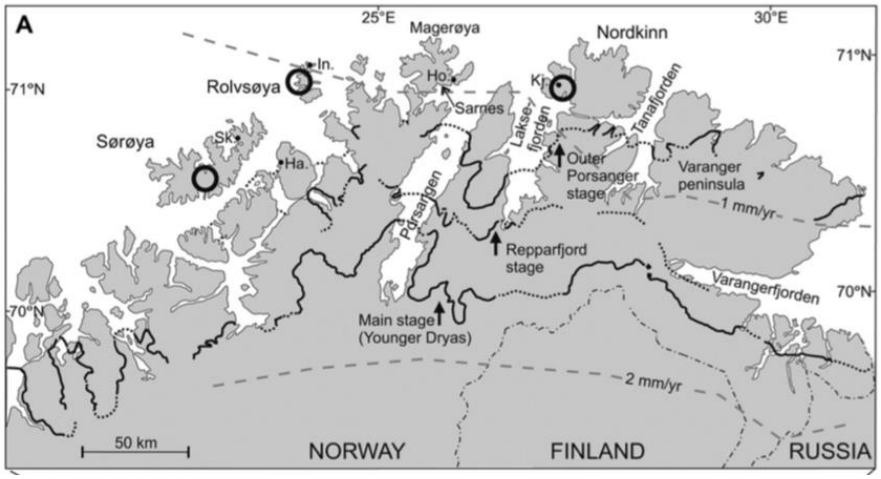

Figure 6. *Locations of postglacial sea level reconstructions from Romundset et al. (2011).*

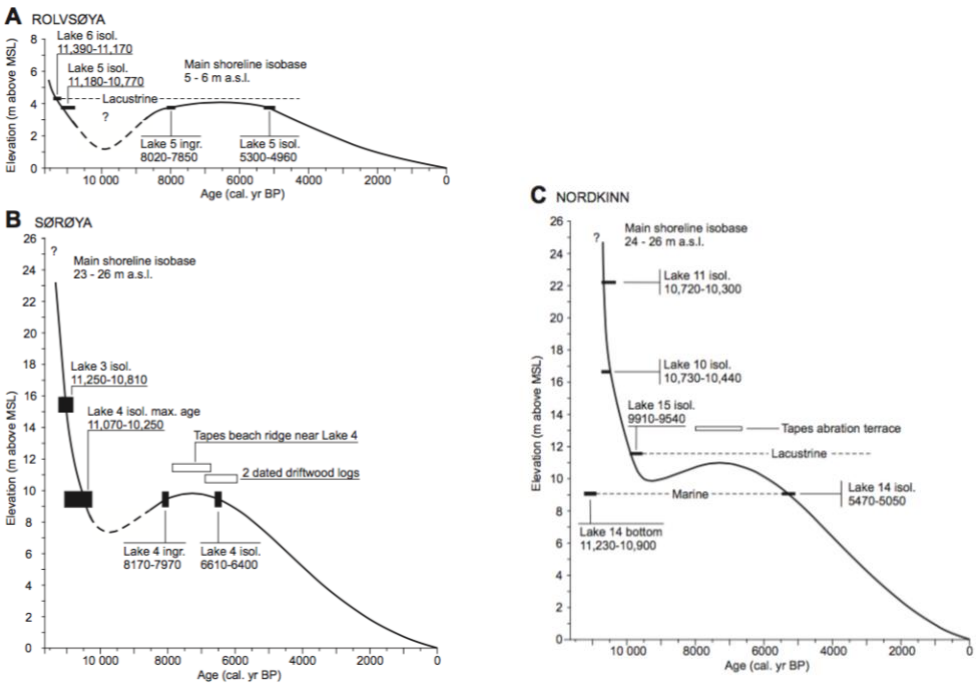

Figure 7. *Reconstructions of postglacial relative sea level on Rolvsøya, Sørøya, and the Nordkinn peninsula. From Romundset et al. (2011).*

It is important to note that isobase patterns drawn from these sea level curves do not match patterns of SIS ice retreat in this region. Additionally, the 4 m asl elevation of the lakes recorded on Rolvsøya do not capture the full extent of the Tapes Transgression. From this work however, the dominant ongoing processes factoring into sea level are observed. Notably, the isostatic uplift following deglaciation is strong and dominates early Holocene sea level. Uplift in each area is not consistent in magnitude, as sea level occurs at different elevations at different locations through time. In the mid and late Holocene, isostatic adjustments decrease but are still present and large enough to bring sea level from the height of the Tapes to where it is today. The source of the Tapes Transgression is not identified through this work, but its presence on the outer coast of Norway is noted.

1.5. Study location: Ingøya, Norway

At 71°N the island of Ingøya, just to the north of Rolvsøya, is located in the Norwegian county of Finnmark (Figure 8). The landscape of Finnmark is deeply indented by the sea with wide fjords, plateaus, and few mountains higher than 600 m (Sollid et al., 1973). On Ingøya the landscape is similar, with plateau styled mountains reaching up to 332 m and lowlands and marine embayments in between. The bedrock geology of Finnmark is generally defined by the boundary of metasedimentary thrust sheets in the north and pre-Cambrian rocks in the south (Corfu et al., 2007; Sturt et al., 1975). Quaternary glacial and marine deposits are overlain by up to a meter of peat and cover the lowlands of Ingøya.

Figure 8. *Arial photograph of Ingøya and northern Rolvsøya.*

1.5.1. Quaternary marine deposits on Ingøya

Postglacial emergence is recorded on Ingøya through series of raised cobble shorelines from 20 to 30 m asl and peat covered sandy shorelines at lower elevations. Marine limit cobble beaches occur at 30 m asl in southwestern Ingøya at the base Mafjordfjellet (Figure 9), while another prominent cobble beach is located at 20 m asl near Kuhelleren. These cobble beaches do not contain any dateable organic material. At 9 m asl, a well-developed peat-covered beach ridge persists across the eastern portion of Ingøya from Sanden Bay to Kuhelleren. Shell fragments can be found in this shoreline, as well as shorelines at lower elevations closer to current sea level. Near Sanden Bay, dune-like landforms exist with shells at the surface. Exposed, shell rich cut banks between Sanden Bay and Østerbotn have associated radiocarbon ages (Savage, 2016). On northern Rølvsoya, shells recovered from several peat-covered raised shorelines have been similarly dated (Mark, 2016). No shorelines are observable from the low-stand in sea level prior to the Tapes Transgression. Lakes on Ingøya range in elevations from 2 – 17.5 m asl. In 2017, the Polar Geospatial Center's sixth release of the open-source Arctic Digital Elevation Model (DEM) provided high resolution mapping for all regions north of 60°, which includes Finnmark and Ingøya. The ArcticDEM can be used to visualize the different morphological features of Ingøya and Rolvsøya and aid in the understanding of relative sea level changes over time.

The purpose of this study is to continue to reconstruct the postglacial emergence of Ingøya, Norway through deriving ages from both raised shorelines and lake sediments in an isolation basin that have formed since the demise of the SIS. From this work, the isostatic uplift pattern of northern Norway can be refined and the retreat of the SIS can be further constrained.

2. Methods

A multi-proxy approach was used to reconstruct postglacial sea level. Marine limit and late glacial raised cobble shorelines were sampled for ^{10}Be exposure ages and considered in conjunction with preexisting radiocarbon dates on bivalves from Tapes shorelines up to 9 m asl (Retelle, unpublished). To constrain the timing of the Tapes Transgression, sedimentary and biomarker transitions indicative of marine and lacustrine conditions were identified in a low-lying basin. Throughout time, low-lying basins such as this have been connected to the sea or isolated from it as a result of changing sea levels. Lakes subjected to such transitions over time are coined 'isolation basins' and have been used in previous relative sea level reconstructions in other high latitude environments (Long et al., 2011). Corresponding radiocarbon dates to these transitions helped constrain the timing of inundation and isolation from rising and falling sea levels through the mid Holocene. Radiocarbon ages and the elevation of the basins's outlet provide a datum to further develop the relative sea level history through the mid Holocene.

Cosmogenic ^{10}Be exposure ages from raised cobbles shorelines were used to date the uppermost 30 m asl marine limit and lower 20 m asl late glacial shorelines. This method of dating has only been used several times in previous sea level reconstructions, but offers a precise means to constrain changes through time (Bierman et al., 2016). The production of ^{10}Be in quartz through cosmic ray bombardment outpaces its 1.39 Ma half-life, which amounts to the net accumulation of ^{10}Be through time on an exposed rock sample. On glacial landforms created since the LGM production of ^{10}Be is essentially linear, while on million year time scales production reaches an asymptote (Ivy-Ochs and Kober, 2008).

Calibration of ^{10}Be concentrations to ages is facilitated through the CRONUS Earth online calculator, which factors in variables such as geographic location, elevation, depth of sample, sample density, production rate, topographic shielding, standards, and erosion rates (Balco et al., 2008). Different scaling schemes of ^{10}Be have been developed to account for the height (or air pressure) of the atmosphere above a sample and time varying effects of earth's magnetic field (Jane et al., 2007). The most prominent approach is the Lal (1991)/Stone (2000) that assumes constant pressure. Additionally, different production rates of ^{10}Be have been established through comparing ^{14}C ages with ^{10}Be concentrations from the same location (Balco et al., 2009; Fenton et al., 2011). CRONUS Earth allows for users to calibrate cosmogenic samples in consistent ways to directly date exposed rock surfaces.

The following sections outline field methods and laboratory methods, and include sampling technique and sample processing for ^{10}Be exposure dating, radiocarbon dating, and a variety of geochemical approaches.

2.1 Field Methods

The field season occurred in two phases during May and August of 2017. In May, raised cobble beaches were sampled for cosmogenic ^{10}Be surface exposure ages and pilot cores were recovered from the isolation basin near Sanden Bay. In August of 2017 the isolation basin was cored once more by Dan Frost, Maddie Mette, and Mike Retelle using a piston coring system. The locations of the isolation basin and the surface exposure sampling sites at the marine limit shoreline and 20 m asl raised cobble shoreline are shown in Figure 9.

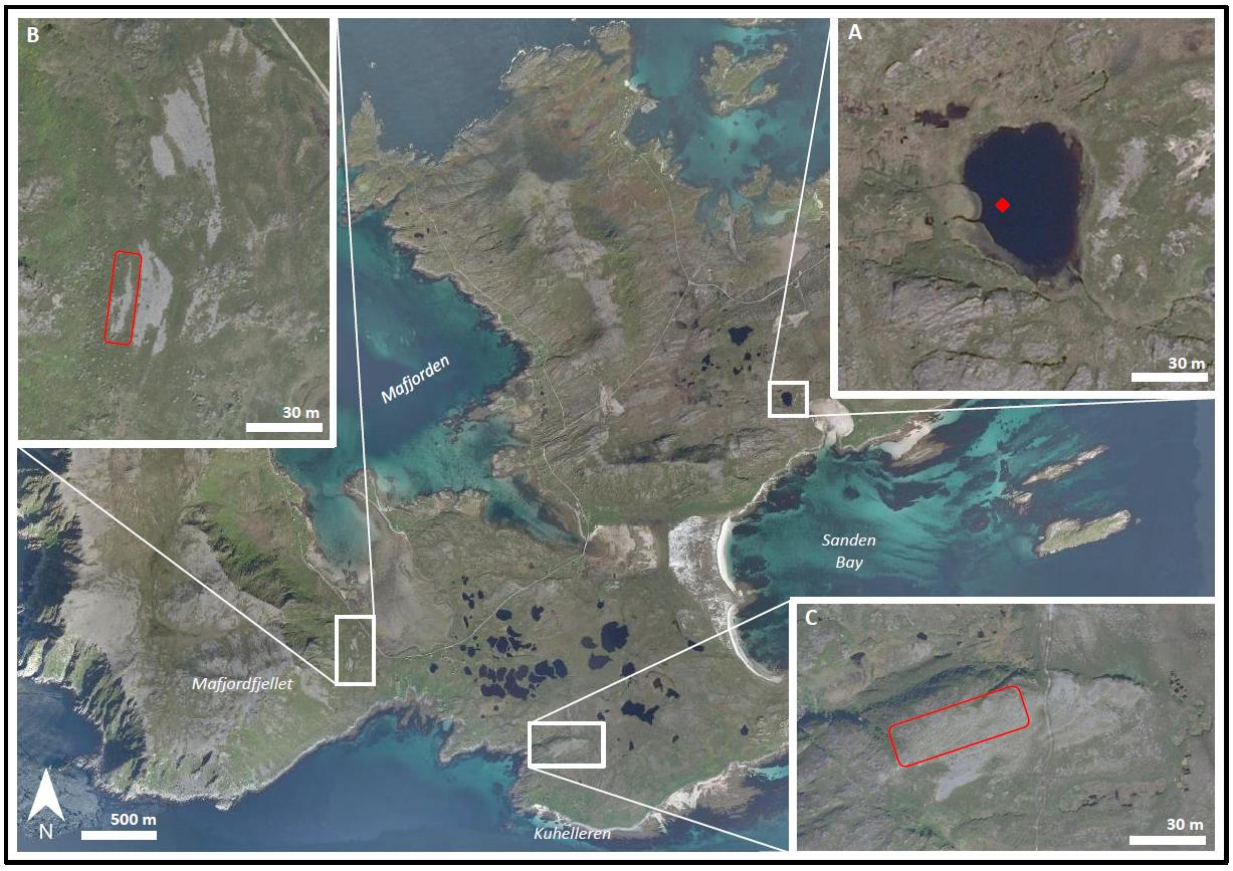

Figure 9. *The location of the isolation basin (A), 30 m asl marine limit (B), and 20 m asl raised cobble shoreline (C). The red diamond indicates the coring location and the red boxes outline the uppermost shorelines were cobbles were sampled. Satellite photographs from Norkart AS © 2017.*

2.1.1. Coring of isolation basin

Sediment cores were recovered in May of 2017 and August of 2017 from the isolation basin at 6 m asl (Figure 10) located at 71°04’02’’ N 24°05’08’’E north of Sanden Bay. In 2016, the bathymetry of the basin was determined with a plumb line (Markonic, 2016) and this reconnaissance was used for locating the coring sites within the basin.

Figure 10. *Photograph of the 6 m asl isolation basin with Sanden Bay and Rolvsøya in the background*

In May of 2017, Livingstone cores L1 and L2 were taken from the deepest point in the lake (1 m) from the platform of an inflatable pontoon raft that was lashed to a 2 x 4 driven into the sediment for stability. All cores taken went to refusal at a sand layer and were archived. In August of 2017 a Vibracorer-adapted Livingstone piston corer was used from the same pontoon raft configuration with the addition of a 2.5 m tripod. The addition of the tripod allowed for the piston in the Livingstone to be anchored above the raft. Two cores obtained were comprised of one long drive and one short drive, the latter of which went to refusal at a sandy gravel layer. Cores were labeled 22.8.17 and 23.8.17.

2.1.2. Surface exposure sampling of raised cobble shorelines

Raised cobble shorelines at 20 m asl and marine limit (30 m asl) were sampled for cosmogenic ^{10}Be exposure ages following the techniques described by Bierman et al. (2016). The 30 m asl marine limit shoreline is located at 71°03’06’’ N 24°00’26’’E and the 20 m asl shoreline is located at 71°02’50’’ N 24°02’39’’E (Figures 11a and 11b). Elevations of all shorelines were surveyed with an auto level and stadia rod. Only the uppermost cobble shorelines at each site were considered for sampling to eliminate the possibility of sampling a reworked cobble from a higher shoreline.

A total of 10 beach cobbles were sampled (Figure 12) with a hammer and chisel: 7 from the 30 m asl marine limit shoreline (C1 - C7) and 3 from the 20 m asl shoreline (C8- C10). Cobbles sampled were chosen based on lack of cover from moss and lichen, stationary appearance, and abundance of quartz. Cobble axes were measured and at least 1 kg from the top 2.5 cm was sampled and bagged. Topographic shielding of the horizon line was measured with the clinometer on a Brunton compass in 30° intervals for 360° around the sample sites.

Figure 11. (a, top) *Photograph of the 30 asl cobble beaches at marine limit at the base of Mafjordjellet. Rolvsøya is shown to the south in the distance.* ***(b, bottom)*** *Photograph of the 20 m asl cobble shoreline on southern Ingøya. The mainland of Finnmark is seen in the distance to the north.*

Figure 12. *Location of the C1 – C7 cobble samples from the marine limit shoreline and C8 – C10 on the 20 m asl shoreline.*

2.2 Laboratory methods

2.2.1 Sediment core laboratory methods

Sediment core preparation

Sediment core tubes L1, L2, 22.8.17, and 23.8.17 were cut lengthwise with heavy duty metal shears and fishing line was used to split the sediment cores into a working half and an archive half. Cores were measured, photographed, and wrapped in plastic and stored in D-tubes in a walk in refrigerator.

Geochemical analysis and magnetic susceptibility

X-ray fluorescence (XRF) studies of marine and lacustrine sediments can determine provenance through high resolution elemental analysis. This technique is commonly applied to a wide range of paleoclimate studies (Croudace and Rothwell, 2015). Downcore elemental profiles of core 23.8.17 were obtained with the Cox ITRAX XRF at the UMass Amherst Geoscience Ronald B. Gilmore XRF Laboratory. The Cox ITRAX XRF is capable of continuous non-destructive analysis of elemental abundance (≥1000 µm) of Al to U, x-ray imagery (≥50 µm), digital imagery (≥500 µm), and magnetic susceptibility (≥2 mm) along sediment cores (http://www.geo.umass.edu/faculty/woodruff/Facilities.html). Sediment core 23.8.17 was scanned on the ITRAX XRF in two sections at 30 kV, 55 mA, and 10 second exposure time with a resolution length of 500 µm and 1000 µm for the long and short sections respectively.

Subsampling for ^{14}C AMS dating and flora identification

Sediment core 23.8.17 was subsampled at 3 cm^3 in 1 cm intervals from depths downcore ranging from 1 – 5 cm, 55 – 60 cm, and 105 – 110 cm. Subsampled sediment was placed in bottles with deionized water, shaken on a vortex genie, then sonicated before being wet sieved at 250 µm for macrofossils. Woody macrofossils were picked with tweezers while the rest of the sediment was dried in beakers.

10 cm^3 of sediment at a depth of 83 cm from core 23.8.17 was wet sieved into 63 – 125 µm, 125 – 250 µm, and >250 µm fractions and subsequently dried. The presence of identifiable flora and fauna was investigated with a stereoscopic microscope. Marine organisms were picked from the subsample and photographed.

Stable isotope and organic matter analysis

Sediment core 23.8.17 was subsampled in 2 cm^3 at 5 cm intervals. Sediment subsamples were freeze-dried to remove all water content. From each sample, approximately 2 mg of organic rich sediment or 30 mg of sand rich sediment was packed into tin capsules with a scapula and a set of tweezers. The mass of the sediment from each subsample was recorded prior to EA-C-IRMS analysis. The mass and corresponding abundance of C and N was converted in to $\delta^{13}C$, C/N, and %C (P. Dostie, pers. comm).

2.2.2 Cosmogenic nuclide laboratory methods

Quartz isolation and ^{10}Be nuclide extraction procedures were done in procedures shown by Corbett et al. (2016). Figure 13 is a flow chart that highlights all the main steps in preparing Be isotopes. ^{10}Be was extracted at the University of Vermont's Cosmogenic Nuclide under the guidance of Lee Corbett of the University of Vermont's Cosmogenic Nuclide Laboratory and Geomorphology Research Group.

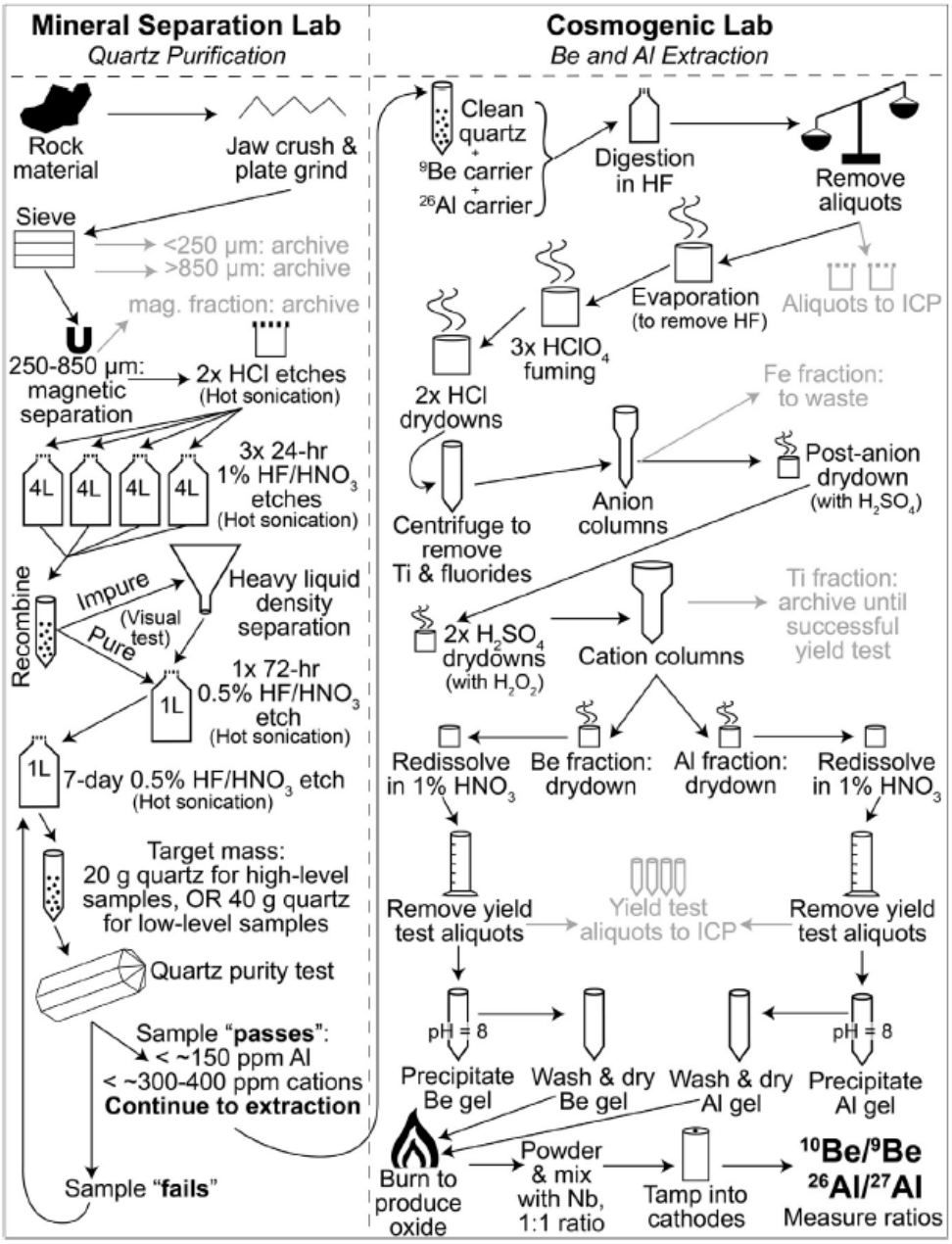

Figure 13. *Corbett et al.'s (2016) flow chart for cosmogenic nuclide extraction. In this study only ^{10}Be in quartz was considered.*

Rock preparation

Samples were crushed in the jaw crusher, ground in the plate grinder, and sieved to 1000 – 250 µm. A small amount of sample was ground in the plate grinder and removed before grinding the majority of the sample to mitigate cross contamination between samples. Sediment >1000 µm and <250 µm was archived. In between each sample run the jaw crusher and plate grinder were cleaned with a vacuum. Sieves were cleaned with a wire brush and

vacuum. The sediment fraction between 250 – 1000 µm was magnetically separated. Between each separation, the magnetic separator was cleaned with a vacuum and a small amount of sample was run to pre-contaminate the machine.

Quartz purification

Concentrated hydrochloric (HCl), hydrofluoric (HF), nitric (HNO_3), and phosphoric acid (H_2PO_4) were used during the quartz purification process. Samples were rinsed in water in a shallow tray to float off micas. Approximately 40 g of sieved and magnetically separated sample was purified through a series of acid etches.

Meteoric ^{10}Be, any dissolved carbonates, or grain-coating oxides were removed through two 24 hour etches with 6N HCL in a 500 ml Teflon beaker. 6N HCl was made by adding 250 ml of 12 M HCl to 250 ml of deionized water. Etches were completed in an ultrasound for sonication and subsequently rinsed three times with deionized water. Once the two HCl etches were complete the samples were dried.

HCl etched samples were etched three times for 24 hours each in 4L of 1% HF/HNO_3 to remove all other minerals except for quartz. 1% HF/HNO_3 was made by adding 50 ml of 16 M HNO_3 and 75 ml of 29 M HF to 4 L of deionized water. Samples were etched in an ultrasound for sonication. Following acid etches, murky water from each bottle was decanted into the sink and the samples were rinsed with deionized water. After the last etch samples were dried in a drying oven. Samples were transferred to 50 mL vials upon drying. Paper shaking of dry samples removed any remaining micas from the pure quartz samples. Once sufficiently clean, samples were etched for 72 hours in 0.5% HF/HNO_3 in 1 L bottles. 0.5% HF/HNO_3 was made by adding 10 ml HF and 5 ml HNO_3 to 1 L of deionized water. Samples were rinsed, etched for one week in 0.5% HF/HNO_3, dried, and massed before quartz purity testing. In all cases, there was >20 g of quartz remaining for each sample after quartz purification.

Quartz purity testing

Inductively Coupled Plasma Optical Emission Spectrometry (ICP-OES) quartz purity testing was completed by Lee Corbett. From samples C1-10, test samples of 0.250 g were transferred to beakers with watch glass lids. Test samples were digested in 5 ml of quartz testing solution (HF/H_2SO_4) on a 95°C hot plate. After one hour at 95 °C, the hot plate was turned to 105 °C for eight hours. Beakers were allowed to cool and as the watch glass lids removed. Hot plates were turned up to 110 °C and the HF was evaporated. Once cooled, 6 ml of Milli-Q water was added to the beakers which were then capped and vortexed. Samples were transferred to ICP tubes and ran on the ICP alongside a standard. Quartz samples with less than 150 ppm Al and <300-400 ppm cations were deemed clean.

Beryllium extraction

Purified quartz samples were processed in the semi-clean Cosmogenic Laboratory for Be extraction (Corbett et al., 2016). All samples were transferred to teflon bottles and massed before adding 250ug ^{9}Be to each sample using beryl carrier produced at University of Vermont with a Be concentration of 291 ug/mL Be. Approximately 100 ml of HF was added to samples saturated with milli-Q water. Samples were digested on a hotplate over several days while increasing the heat up to 135°C gradually. A blank was made with 250 µm of the ^{9}Be carrier.

Aliquots representing 2 – 4% by mass of each sample were added to ICP beakers. 25 µl of H_2SO_4 was added to the aliquots to prevent samples from drying out during HF evaporation. 5 ml of Ga/Y spiked weak H_2SO_4 was added to the aliquots. These aliquots were analyzed on the ICP-OES for high-precision quantification of total Be and Al.

Fluoride compounds in samples were driven off through a series of three perchloric acid (2 ml $HClO_4$) dry-downs on a hotplates set at 230°C. Samples were converted to chloride form through two concentrated hydrochloric acid (2ml HCl) dry-downs on a hotplate set at 160°C. Samples were centrifuged to remove Ti. Fe in samples was removed through anion column chromatography while cation column chromatography removed B and Ti and separated Be from Al. Samples were dissolved again in 1% nitric acid (8 ml HNO_3) on a hotplate at 60°C. Samples were transferred to acid-washed capped tubes. Yield aliquots, composed of 200 µl of sample with 5 ml H_2SO_4, were removed for ICP-OES analysis. Beryllium hydroxide was precipitated with 30% NH_4OH and a methyl red indicator, stopping once a pH of 8 was reached. Sample tubes were vortexed and liquid was dried on a hotplate at 65°C until all that remained was a pellet. The pellet was burned with a gas flame, mixed in a 1:1 ratio with Nb, and packed into steel cathodes for AMS analysis.

2.2.3 Accelerator Mass Spectrometry

Accelerator mass spectrometry (AMS) is method of detecting low concentrations (10^{-12} – 10^{-16}) of stable and unstable isotopes (Hellborg and Skog, 2008). As a result, AMS only requires samples to be of mg or sub-mg size (Hellborg and Skog, 2008). For radiocarbon dating, organic material from sediment core 23.8.17 was sent to the Woods Hole NOSAMS dadiocarbon dating laboratory. AMS was used to determine the $^{14}C/^{12}C$ ratio in each sample. For cosmogenic exposure dating, beryllium cathodes were sent to the Purdue PRIME laboratory for $^{10}Be/^{9}Be$ ratio determination. Ratios were normalized to standard 07KNSTD with an assumed ratio of 2850 x 10^{-15} (Nishiizumi et al., 2007).

2.2.4 Age Calibration

^{14}C age calibration

Radiocarbon ages were calculated with the following relationship (WHOI, n.d.):

$$F = \frac{14C}{12C}$$

$$Age \ = \ -8033 \ ln(F).$$

Here, F is the ratio between atoms of ^{14}C and ^{12}C. The IntCal13 calibration curve was used to calibrate terrestrial samples (Reimer et al., 2013). Calibrations were performed with the CALIB 7.1 online calculator by Stuiver et al. (2017).

^{10}Be age calibration

Cosmogenic beryllium ages were calculated with the CRONUS-Earth online calculator v2.2 (https://hess.ess.washington.edu/) with the North East North America ^{10}Be production rate (Balco et al., 2008)(Balco et al., 2009). The Lal (1991) and Stone (2000) altitude and latitude scaling theme (St) of constant spallogenic ^{10}Be production was used in calibration. The ^{10}Be half-life of 1.39 Ma and decay constant of 4.62 x 10^{-7} yr^{-1} were used (Balco et al., 2008). The topographic shielding, geographic location, elevation, and sample thickness of 2.5 cm where taken into consideration when calibrating. No correction for snow cover or erosion was implemented in calibration.

2.3. DEM Sea Level Projections

GIS sea level projections for marine limit and Tapes shorelines were done using the Polar Geospatial Center's ArcticDEM. Local strip DEM files covering Ingøya and Rolvsøya were retrieved with the ArcticDEM Strip Index on ArcMAP. The raster strip file was manipulated to compensate for isostatic tilt according to Newton's (2002) established protocol for glacial Lake Hitchcock (https://d32ogoqmya1dw8.cloudfront.net/files/NAGTWorkshops/gis/activities/student_handout_lake_hitchcock.pdf). Gradients of 2.3 m km^{-1} and 0.2 m km^{-1} where applied from north to south to the DEM for marine limit and Tapes sea level projections, respectively. In each projection, a hillshade was applied to the tilt corrected DEM to provide topographic relief. The logical commands of the raster calculator were used to define the elevation of inundation on the DEM, and the resulting raster was converted to a polygon feature to project sea level in relation to the surrounding landscape. The following steps outline this methodology:

1. Con(IsNull(dem),0,dem) = new raster
2. SetNull(new raster > sea level, 0) = inundated area
3. Raster converted to polygon.

3. Results

3.1 Cosmogenic ^{10}Be surface exposure dating

Surface exposure samples C1 – 7 from the 30 m asl marine limit shoreline and C8 – 10 from the 20 m asl shoreline record deglaciation and postglacial uplift of the region. Table 1 gives sample collection data and the resulting cosmogenic ^{10}Be concentrations and uncertainties derived from the ^{10}Be/^{9}Be atomic ratio (see Appendix A for the corresponding results). Samples C1 – 7 yielded ^{10}Be concentrations ranging from 5.97 x 10^4 – 7.95 x 10^4 atoms g^{-1}, correlating to ages ranging from 14.0 – 18.7 ka for the 30 m asl shoreline (Table 1). Cosmogenic ^{10}Be concentrations of samples C8 – 10 from the 20 m asl shoreline range from 6.30 x 10^4 – 7.27 x 10^4 atoms g^{-1} and date to 14.6 – 16.8 ka (Table 1). Figures 14 and 15 show plots of the probability density functions for samples C1 – 7 and C8 – 10 (Corbett, pers comm). Samples C1 and C10, dating to 18.7 ka and 16.8 ka respectively, are considered outliers due to inherited ^{10}Be and their deviation from the central population of ages. The average age and uncertainty (±1 σ) of samples C2 – 7 is 14.8 ± 0.5 ka while for samples C8 – 9 it is 14.8 ± 0.3 ka.

The exposure age on the uppermost 30 m asl boulder beach (n=6) of 14.8 ± 0.5 ka provides an estimate for the formation of the marine limit shoreline and initial postglacial emergence and a minimum estimate for deglaciation of the northern Norwegian coast. Although the average ages of the 20 m asl and 30 m asl shorelines are indistinguishable, the uncertainties of ± 0.3 ka and ± 0.5 ka provide a range of ages for the formation of the two shorelines.

Sample	Elevation (m asl)	Latitude (°N)	Longitude (°E)	Thickness (cm)	Shielding	^{10}Be conc. (atoms/g)	^{10}Be unc. (atoms/g)	^{10}Be age (ka)	^{10}Be age unc. (ka)
C1	30	71.051861	24.006944	2.5	0.9748	7.95×10^4	3.27×10^3	18.7	0.8
C2	30	71.051778	24.006944	2.5	0.9748	6.52×10^4	2.56×10^3	15.3	0.6
C3	30	71.051778	24.006944	2.5	0.9748	6.16×10^4	2.30×10^3	14.5	0.5
C4	30	71.051722	24.006667	2.5	0.9748	5.97×10^4	2.17×10^3	14.0	0.5
C5	30	71.051611	24.006667	2.5	0.9748	6.34×10^4	2.26×10^3	14.9	0.5
C6	30	71.051722	24.006944	2.5	0.9748	6.26×10^4	2.30×10^3	14.7	0.5
C7	30	71.051806	24.006944	2.5	0.9748	6.50×10^4	2.19×10^3	15.3	0.5
C8	20	71.047028	24.044167	2.5	1	6.30×10^4	2.23×10^3	14.6	0.5
C9	20	71.047028	24.044167	2.5	1	6.49×10^4	2.68×10^3	15.0	0.6
C10	20	71.046722	24.044167	2.5	1	7.27×10^4	2.72×10^3	16.8	0.6

***Table* 1.** *Surface exposure sample collection and laboratory data and the corresponding ages. Ages are calculated with CRONUS Earth v.2.2., NENA production rate, Lal/Stone scaling.*

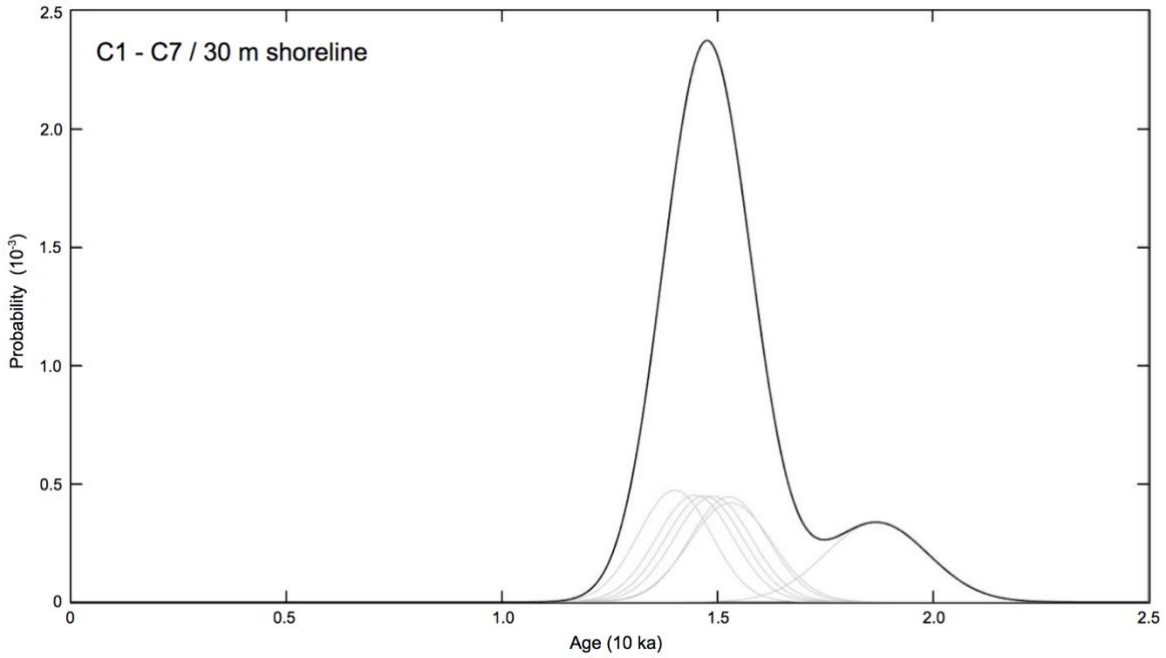

Figure 14. *Plot of the probability density function for samples C1 – 7. The average age under the main peak is 14.8 ± 0.5 ka.*

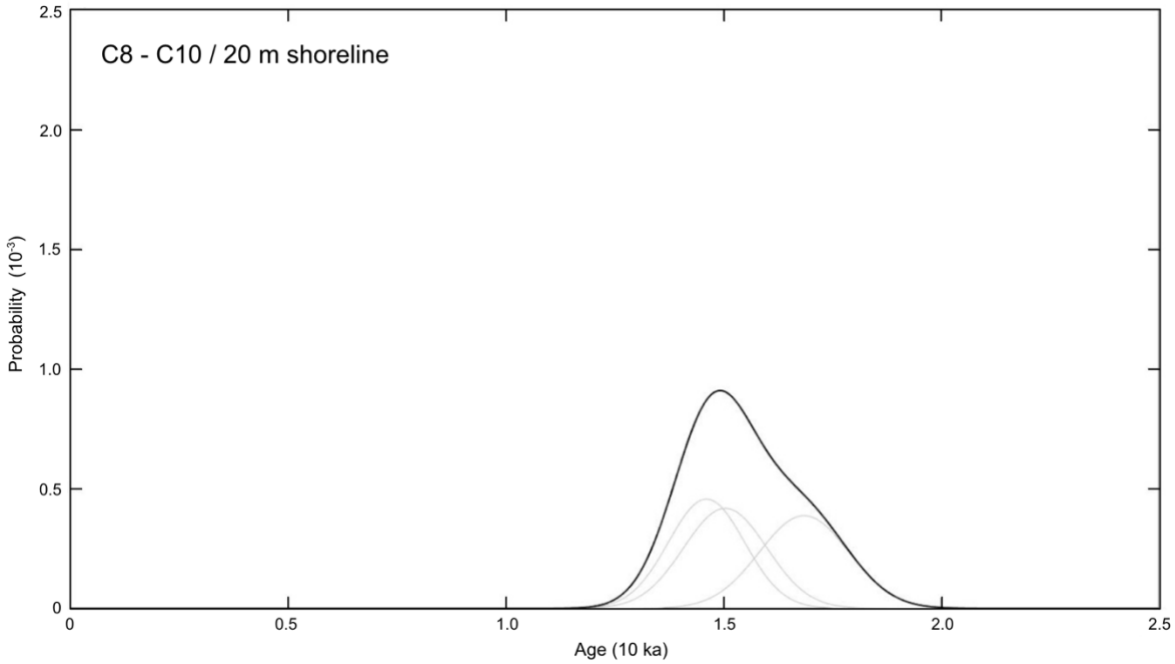

Figure 15. *Plot of probability density function for samples C8 – 10. The average age under the main peak is 14.8 ± 0.3 ka.*

3.2. Isolation basin sedimentary record

A composite stratigraphic log of sediment core 23.8.17 is comprised of five primary units identified in Figure 16 and described in the following sections.

Unit 1

Sediment from 0 – 55 cm is dark brown in color, fine grained, organic rich, and possesses thin, (≤1 cm) lighter colored laminae of sand at 6 cm and 20 cm. A woody macrofossil from 3 – 4 cm has a maximum age of to 667 ± 5 cal yr BP (Table 2), indicating low sedimentation rates around 0.005 cm yr^{-1} or the incorporation of an old, terrestrial woody fragment due to overland flow.

Unit 2

From 55 to 99 cm, unit 2 is distinguished as orange-brown, organic rich sediment with a higher abundance of mica. Unit 2 is more oxidized than unit 1, and this is seen through a change from dark brown gytia in unit 1 to denser orange-brown sediment in unit 2. Macrofossils in unit 2 include fragments from woody terrestrial plants and submerged aquatic vegetation. Woody macrofossils in this zone are dated to 5056 ± 15 cal yr BP and 5318 ± 5 cal yr BP (Table 2). Fragments of what is likely the eelgrass *Zostera marina* were found at 83 cm (Figure 17). EA-C-IRMS analysis of 2.12 µmol of *Zostera marnia* for $\delta^{13}C$ and %C yielded -26‰ and 30.38%, respectively.

Unit 3

The oscillatory zone between 99 and 112 cm, defined as unit 3, is characterized by alternating layers of sand and organic rich sediment. Thin, fine grained sand layers at 99 – 100 cm, 107 – 108 cm, and 109 – 111 cm separate sequences of denser lacustrine sediment. This zone has a maximum age of 7590 ± 20 cal yr BP.

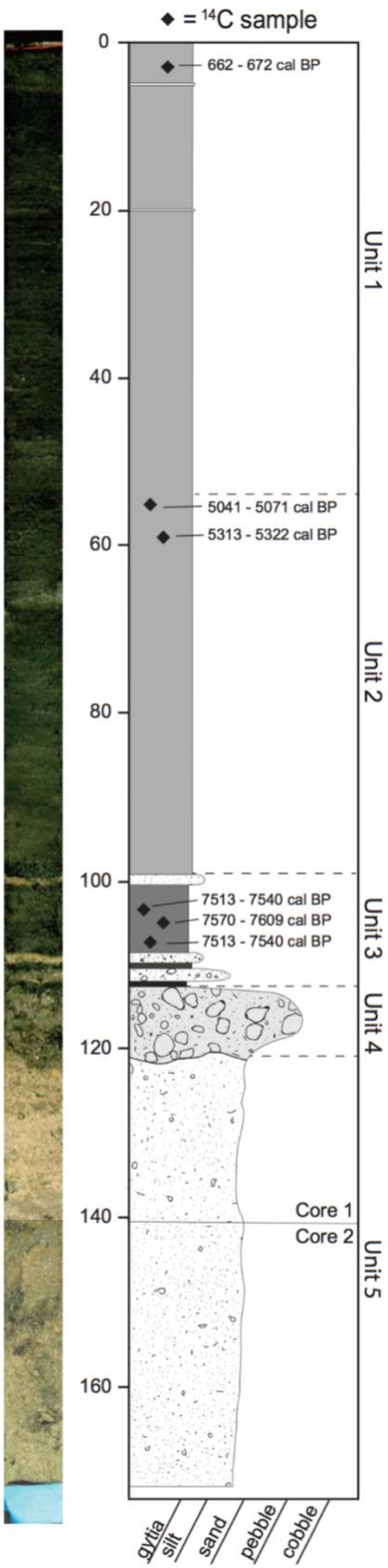

Figure 16. *Optical photograph and sediment log of the two consecutive cores (core 1 from 0 – 140 cm, core 2 from 140 – 171 cm) from the isolation basin.*

Unit 4

Unit 4 is from 112 to 120 cm and is comprised of dark grey sandy gravel with angular clasts >3 cm. No organic matter was found in this unit. A distinct transition in sediment size, lithology, and color at 120 cm marks the end of this unit.

Unit 5

From 120 – 171 cm, unit 5 is a sequence of sand with small rounded gravel clasts of ~1 cm in size. Throughout unit 5 there is no observable organic matter. The bottom of the aluminum core tube from core 2 was bent, likely due to the presence of larger cobbles below.

Depth (cm)	^{14}C Age	^{14}C Age Error	Age Range cal BP	Age cal BP avg.	Age cal BP unc.
3-4	700	15	662 - 672	667	5
56-57	4,470	30	5041 - 5071	5056	15
59-60	4,620	20	5313 - 5322	5318	5
106-107	6,670	25	7513 - 7540	7527	14
107-108	6,720	30	7570 - 7609	7590	20
108-109	6,670	25	7513 - 7540	7527	14

Table 2. *AMS ^{14}C and cal yr BP ages for sediment core woody macrofossils.*

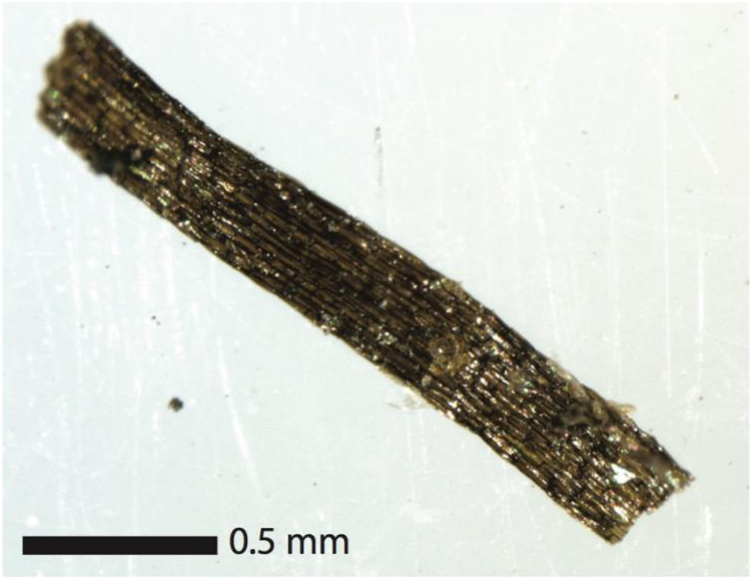

Figure 17. Photograph of the eelgrass *Zostera marina* found at 83 cm in unit 2.

3.3. Isolation basin geochemistry

ITRAX XRF analysis of the sediment cores produced a sedimentary geochemical profile of the elements from Al to Dt. The corresponding file of all downcore elemental data is presented in Appendices B and C. The elemental profiles of K, Ca, Ti, and Fe are presented in Figure 18. In units 1 and 2 both K and Ca are at baseline values near 0 counts, below which in units 4 and 5, there is shift to an elevated signal from 108 – 171 cm coincident with the change to the basal, sandy sediments. Ti shifts from baseline values further downcore at 112 cm. Fe is present in the sediment throughout the core; however there is an increase at 64 cm from lower to higher values when moving from unit 1 to unit 2.

Analysis of δ^{13}C, C/N, and %C give insight to the provenance of sedimentary organic matter (Figure 19). Sedimentary δ^{13}C ranges from -28.85 to -21.76‰ from the top to the bottom of the core. Constant values of approximately -28‰ in unit 1 are indicative of a terrigenous, C3 plant source of sedimentary organic matter. In unit 2, δ^{13}C becomes enriched by approximately 3‰ possibly due to influence of an increase in submerged aquatic vegetation (SAV) in addition to terrigenous organic matter. Downcore δ^{13}C content is more enriched reaching -21.76‰ at 170 cm. Average δ^{13}C values in unit 1 are -28.62‰, in unit 2 are -26.88‰, and in unit 5 cm are -24.06‰. C/N ratios down core are mostly constant in the top 115 cm, while below this the ratio decreases. Average C/N ratios in units 1 and 2 and in unit 5 cm are 20.75 and 9.83, respectively. This shift reflects the transition from terrigenous organic matter in the lacustrine sediments to a mixed terrestrial and SAV signal to a marine phytoplankton signal downcore. Percent carbon (%C) down core is highly variable in the lacustrine sediment and almost 0% throughout units 4 and 5. Average %C is 19.59 in units 1 and 2, while in units 4 and 5 average %C is 0.11. These results are not necessarily *organic carbon*, but it is assumed that organic carbon makes up most of the carbon derived from EA-C-IRMS of the sediments. This assumption is based upon the siliceous rocks and the lack of carbonate in the isolation basin sediments.

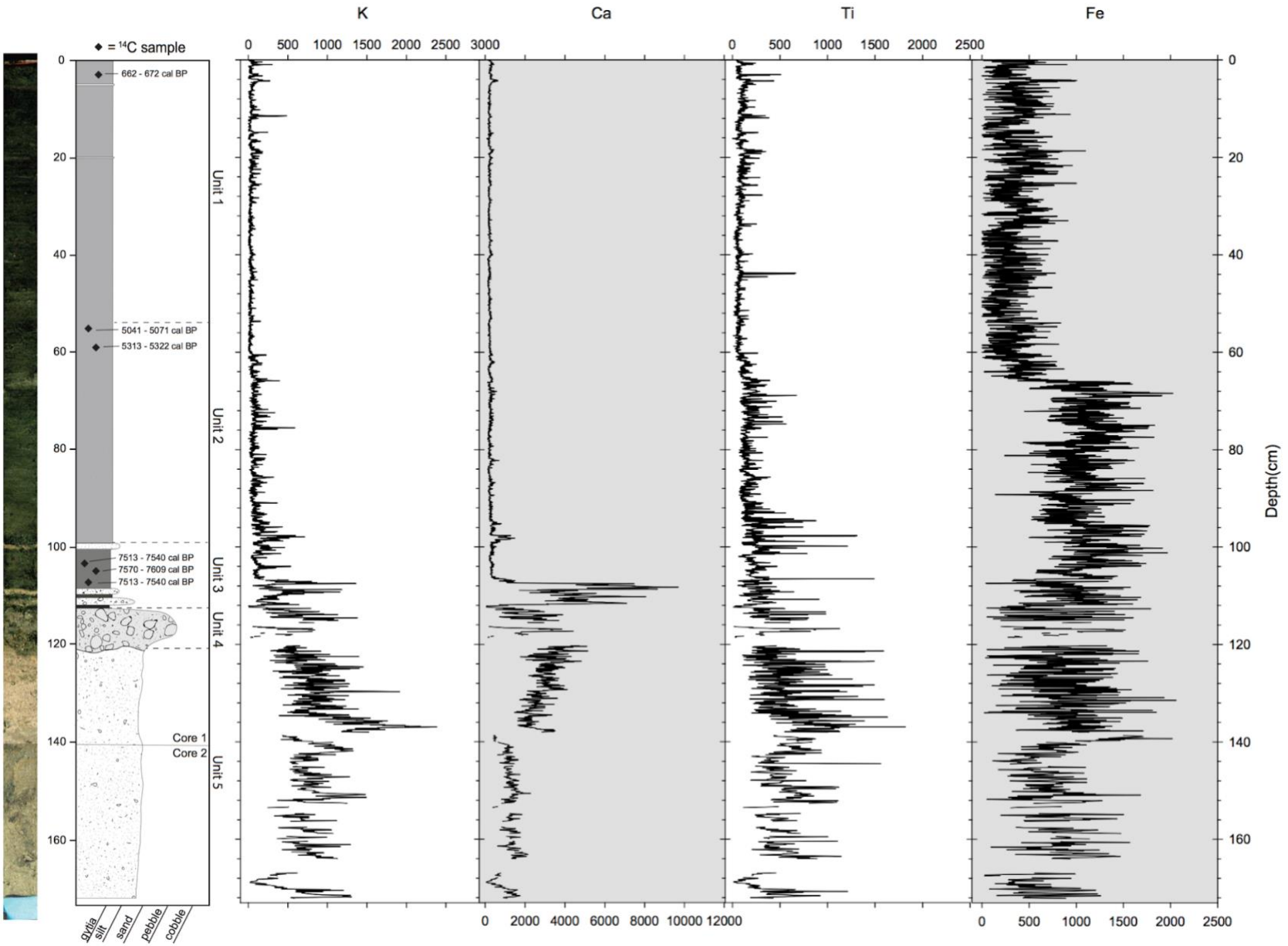

Figure 18. *ITRAX XRF down core plots of K, Ca, Ti, and Fe. Note the shifts at 110 cm for K and Ca, ~95 cm for Ti, and 65 cm for Fe.*

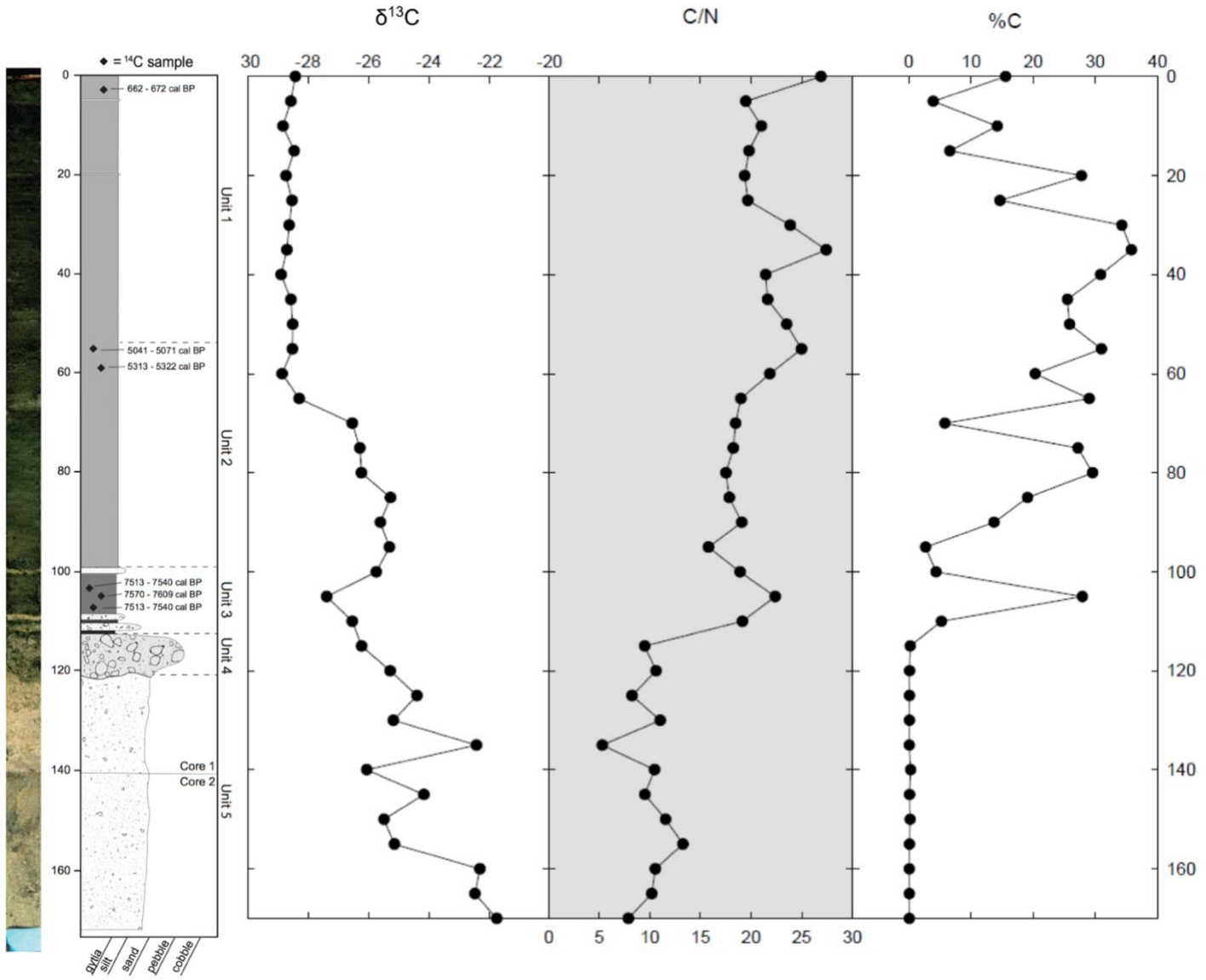

Figure 19. *Down core plot of $\delta^{13}C$, C/N, and %C. Note the two distinct shifts in $\delta^{13}C$ at 60 cm and 120 cm, and in C/N at 120 cm. At 120 cm, %C is nearly 0% due to sandy sediment.*

4. Discussion

4.1. Deglaciation of the north coast

Dated offshore and onshore glacial deposits constrain the timing of deglaciation of the Barents Sea and the northern Norwegian coast following the last glacial maximum (Landvik et al., 1998; Romundset et al., 2017; Winsborrow et al., 2010). Reconstructions based upon seismic surveys and ^{14}C dates on bivalves suggest that deglaciation of the Barents Sea was complete by 15 ka, with ice streams facilitating ice sheet retreat (Hughes et al., 2016; Winsborrow et al., 2010). Throughout the Barents Sea, bivalves found both in till and marine sediment give maximum and minimum constraining ages for deglaciation, respectively. Minimum ages of ca. 14,100 – 15,600 cal yr BP and 13,300 cal yr BP have been reported on bivalves in marine mud overlying till approximately 100 km to the north of Ingøya in the southern Barents Sea. Maximum ages from shells and shell fragments in till/diamicton in this same region range from 20,000 – 30,000 cal yr BP (Landvik et al., 1998; Winsborrow et al., 2010). See Figure 20 for the spatial relationship between these ages. To the southwest near Andøya, the submarine Egga moraine systems are dated to ca. 18 ka (Mangerud, 2004).

The 14.8 ± 0.5 ka cosmogenic ^{10}Be age of the marine limit shoreline on Ingøya, which is contemporaneous with deglaciation, is consistent with the regional ages. To the south on Rolvsøya, an isolation basin basal sediment core ^{14}C age of 14,790 – 13,860 (±2 σ) cal yr BP from a *Mya truncata* shell complements the surface exposure age from marine limit (Romundset et al., 2011). This age is a minimum age, as a *Mya truncata* would only inhabit this environment after the SIS had retreated from it. Since the *Mya truncata* shell is a minimum age, it is likely that deglaciation of Ingøya and Rolvsøya occurred at the upper limit of these two ages. Together, these ages provide further constraint for deglaciation of the north coast and mark the termination of the SIS's marine-based ice margin in this region.

Dated recessional moraines inland (south) from Rolvsøya and Ingøya further contextualize the deglaciation chronology (Figure 20). The outermost moraine system mapped by Sollid et al. (1973) is dated to 15,000 – 14,000 ^{14}C yr (Andersen, 1979). Romundset et al. (2017) dated the moraines of the Outer Porsanger and Tromsø-Lyngen sub-stages that are prominent throughout Finnmark (Figure 4). Surface exposure ages of 14.6 ± 1.7 ka and 13.6 ± 1.4 ka were obtained for Outer Porsanger sub-stage while an age of 11.2 ± 1.2 ka was determined for the Tromsø-Lyngen sub-stage (±2 σ, CRONUS v.2.2, scaling production rate). Recalibration of ^{10}Be concentrations used in Romundset et al.'s (2017) study with the NENA production rate and Lal/Stone scaling on CRONUS Earth v.2.2 allowed for a consistent comparison with the surface exposure ages from Ingøya. Ages of 14.9 ± 0.1 ka (n=3) and 14.4 ± 0.2 ka (n=3) (±1 σ) for the Outer Porsanger moraine are in agreement with the 14.8 ± 0.5 ka age from marine limit on Ingøya (approximately 50 km to the north). The Tromsø-Lyngen sub-stage

recalibration resulted in an age of 12.6 ± 0.7 ka, consistent with previous reconstructions aligning the Tromsø-Lyngen sub stage with the 12.7 ka Younger Dryas ice margin (Andersen, 1965; Marthinussen, 1962; Stroeven et al., 2016). This moraine system is correlated with the Main shoreline (Andersen, 1965; Sollid et al., 1973), which has implications for the relative sea level history of the outer north coast.

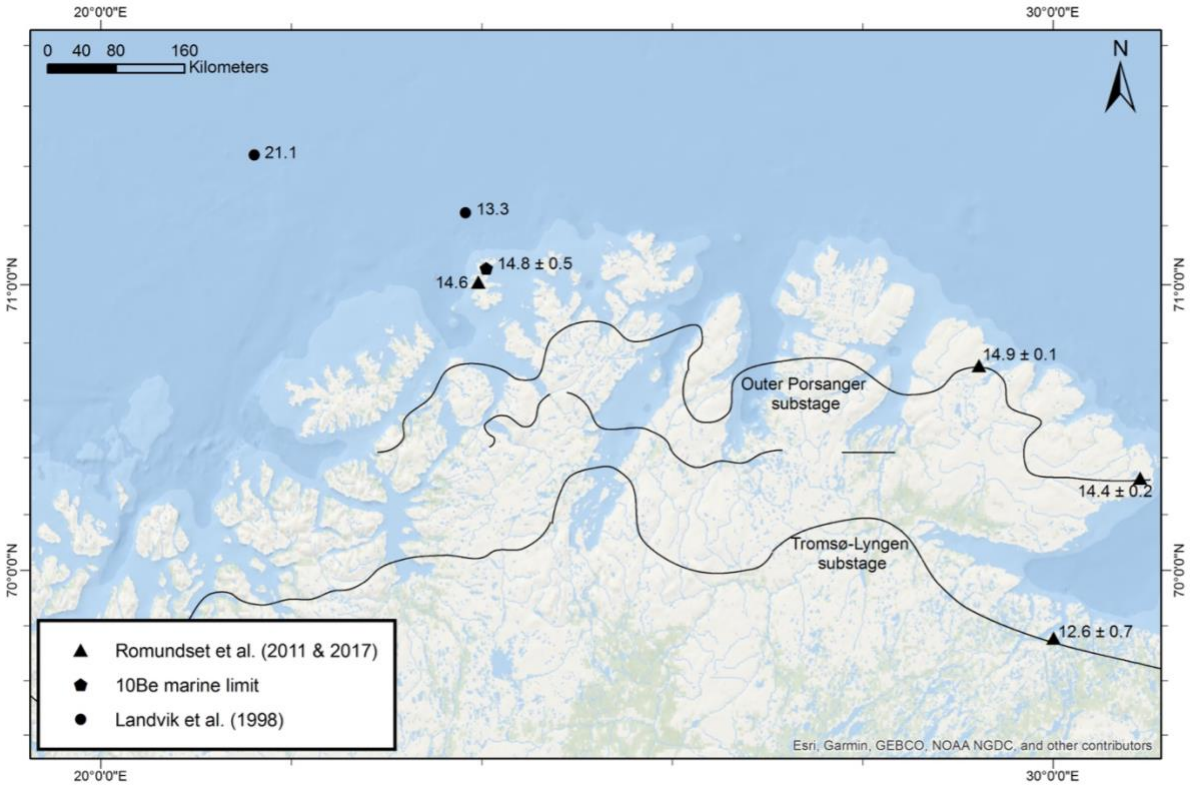

Figure 20. *Spatial relationship of ^{14}C ages of marine bivalves found in till and marine sediment (Landvik et al, 1998). On Rolvsøya, Romundset et al.'s (2011) basal ^{14}C age is in agreement with the ^{10}Be age of the 30 m asl marine limit shoreline. Approximate glacial sub stages from Romundset et al. (2017) are shown inland.*

4.2. Relative sea level history

Ingøya and Rolvsøya experience similar postglacial isostatic adjustments and changes in ocean water volume through time. Provisional relative sea level curves for both locations can be seen in Figure 21a and 21b, while Figure 21c illustrates the driving forces behind these changes. Since Rolvsøya is located slightly south of Ingøya, synchronous shorelines appear slightly higher than they do on Ingøya. On the Ingøya curve, the relative sea level history is defined by cosmogenic ^{10}Be dated beach cobbles (red), radiocarbon-dated woody macrofossils from the 6 m isolation basin (black), and marine bivalves on raised beaches from and below the uppermost Tapes shoreline (green). The provisional relative sea level curve from northeastern Rolvsøya is comprised of isolation basin ^{14}C ages (black, from Romundset et al., 2011) and low precision AMS radiocarbon ages on marine bivalves from raised beaches (red). The 45 m asl marine limit elevation on northeastern Rolvsøya is from Marthinussen (1960).

Since deglaciation of the outer north coast of Norway at 14.8 ± 0.5 ka, the dynamics between isostatic processes and eustatic processes have been main the driving factors behind the postglacial sea level history (Figure 21c). Their significance through time varies, with initial isostatic uplift initially outpacing eustatic rises in sea level from the melting of the worlds ice sheets. The early Holocene relative low stand in sea level remains unconstrained. However, its presence is likely due the continued uplift of the curst in combination with the crustal forebulge from the SIS (Barnhardt et al., 1995). The potential collapse of the forebulge and meltwater from the continued melting of the world's ice sheets – namely the Antarctic Ice Sheet – led to the approximate 9 m of sea level rise during the Tapes Transgression. Thereafter, eustatic sea level rise was outpaced by residual isostatic uplift of Scandinavia and the outer north coast, ultimately bringing sea level to where it is today. Figure

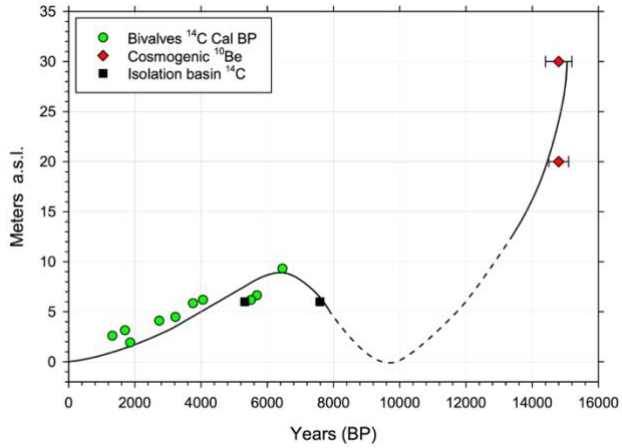

Figure 21a. Postglacial relative sea level curve for Ingøya, Norway. Bivalve ^{14}C ages (Retelle, unpublished) are considered as the maximum limit of sea level in most cases due to the possibility of their transport to higher shorelines during storm events. Sediment core ages from the Ingøya isolation basin constrain sea level during the Tapes Transgression.

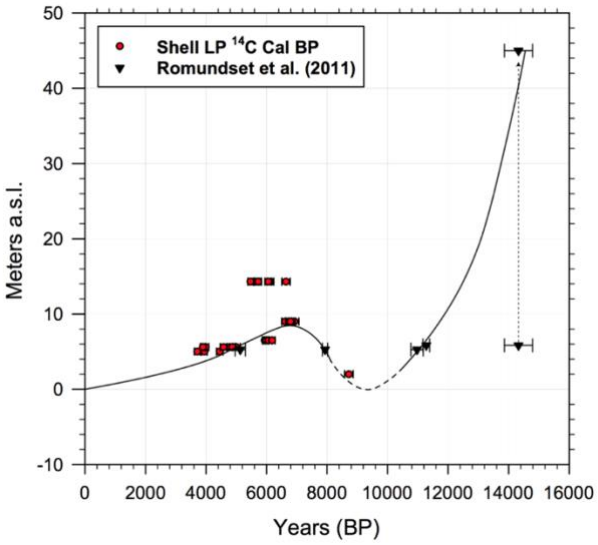

Figure 21b. *The relative sea level curve for Rolvsøya is constrained by low precision AMS ages on bivalves (Retelle, unpublished) as well as isolation/inundation events for lakes at 5.23 and 5.80 m asl (from Romundset et al., 2011).*

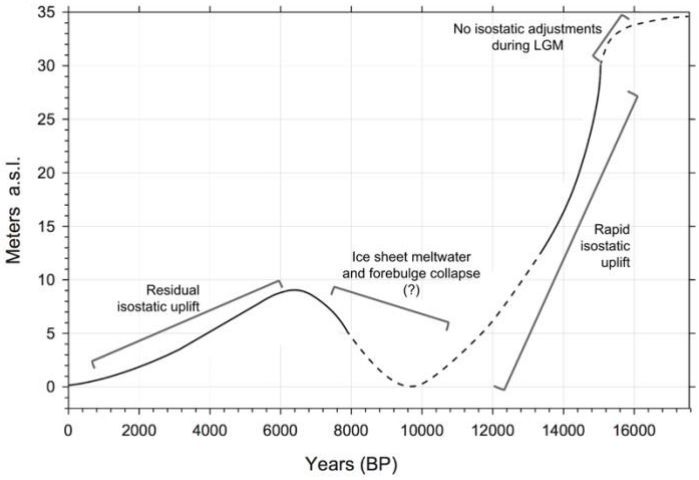

Figure 21c. *The driving forces behind the relative sea level history of the outer north coast of Norway vary through time. Brackets and illustrate when isostatic or eustatic processes dominate.*

Differential isostatic uplift following deglaciation has resulted in the tilt of contemporaneous shorelines from Ingøya to Rolvsøya. The calculated tilt from north to south of the marine limit shoreline is 2.3 m $km^{-1}$and the Tapes Shoreline is 0.2 m km^{-1}. Although the Main Shoreline is not observable at this location on the north coast due to the early Holocene low stand in sea level, it is estimated from Marthinussen (1960) that the isostatic tilt is 1 m km^{-1}. The schematic in Figure 22 depicts the relationship between shoreline elevations and distance, which is used to correct the ArcticDEM for more accurate sea level projections (Figures 23 – 25).

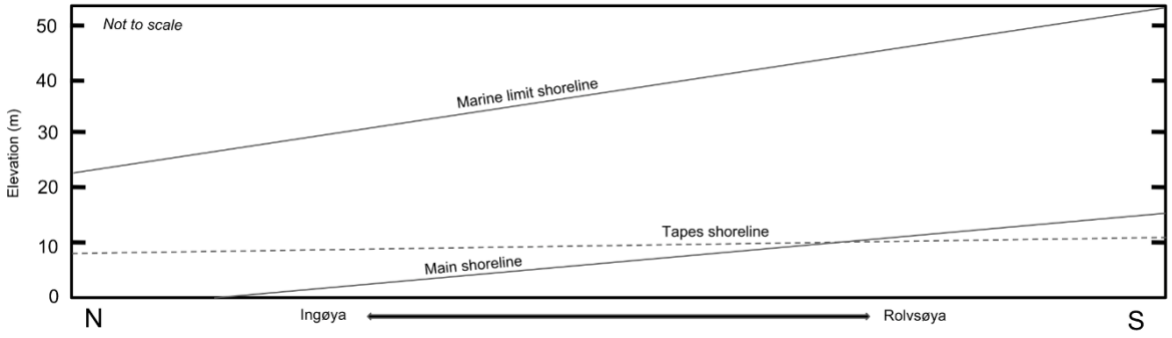

Figure 22. *Shoreline tilt diagram derived from the relative sea level curves for Ingøya and Rolvsøya.*

4.2.1. Marine limit – ca. 14.8 ka

Synchronous ca. 14.8 ka marine limit shorelines on both Ingøya and Rolvsøya are marked at 30 m and 45 m, respectively. Sea level projections on the shoreline-tilt-corrected ArcticDEM delineates marine limit across both of islands. Marine limit on the outer north coast is much lower than it is both to the south and to the east in northern Scandinavia. On both the Kola Peninsula far to the east and 200 km to the south west, marine limit shorelines are consistently at approximately 60 m (Evans et al., 2002; Snyder et al., 1996). A lower 20 m shoreline on Ingøya is dated to 14.8 ± 0.3 ka, suggesting a rapid fall in relative sea level due to rapid initial postglacial isostatic uplift of the outer coast of Finnmark. Considering the uncertainty associated with the ^{10}Be ages, uplift rates range from 1.5 – 3 m per century from 15.1 – 14.4 ka. On Rolvsøya, approximate uplift rates from 14.6 – 11.28 ka are 1.2 m per century (Romundset et al., 2011). The slight difference between these rates can be attributed to the difference in the time span these averages are taken over. Since isostatic uplift rates decrease with time, a lower average for Rolvsøya is expected. Moreover, these postglacial isostatic uplift rates are similar to those elsewhere in Norway. To the south in Bergen, the relative sea level history is well constrained. Uplift rates are calculated to be approximately 1.7

m per century in the early Holocene over a time period with equidistant ice margin retreat when compared to northern Norway from 14.6 – 11.5 ka (Wohlfarth et al., 2008).

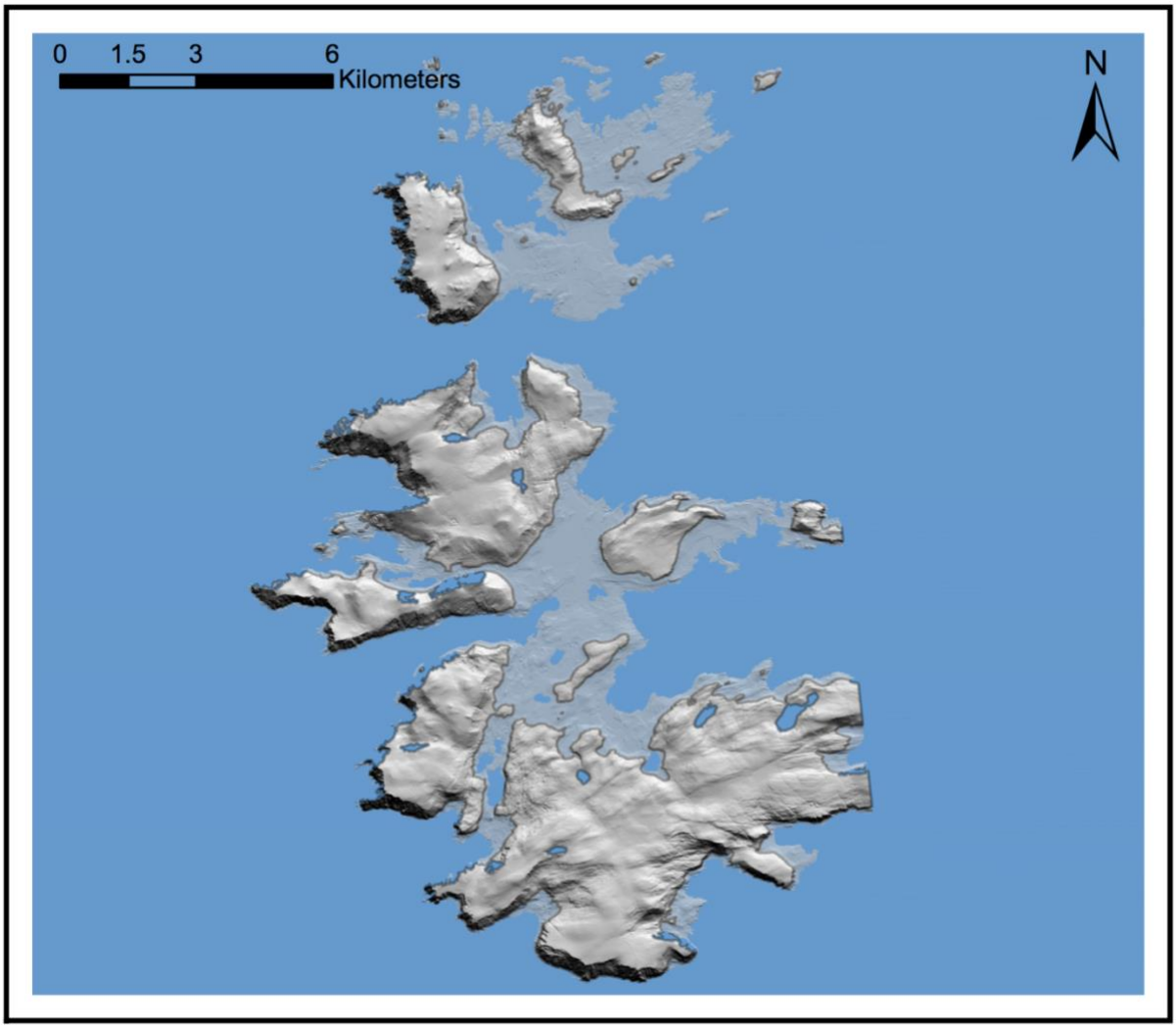

Figure 23. *Marine limit sea level projection with an isostatic tilt correction of 2.3 m km-1. Modern day inundated landscape is shown in light gray/blue while the marine limit is marked by the grey line.*

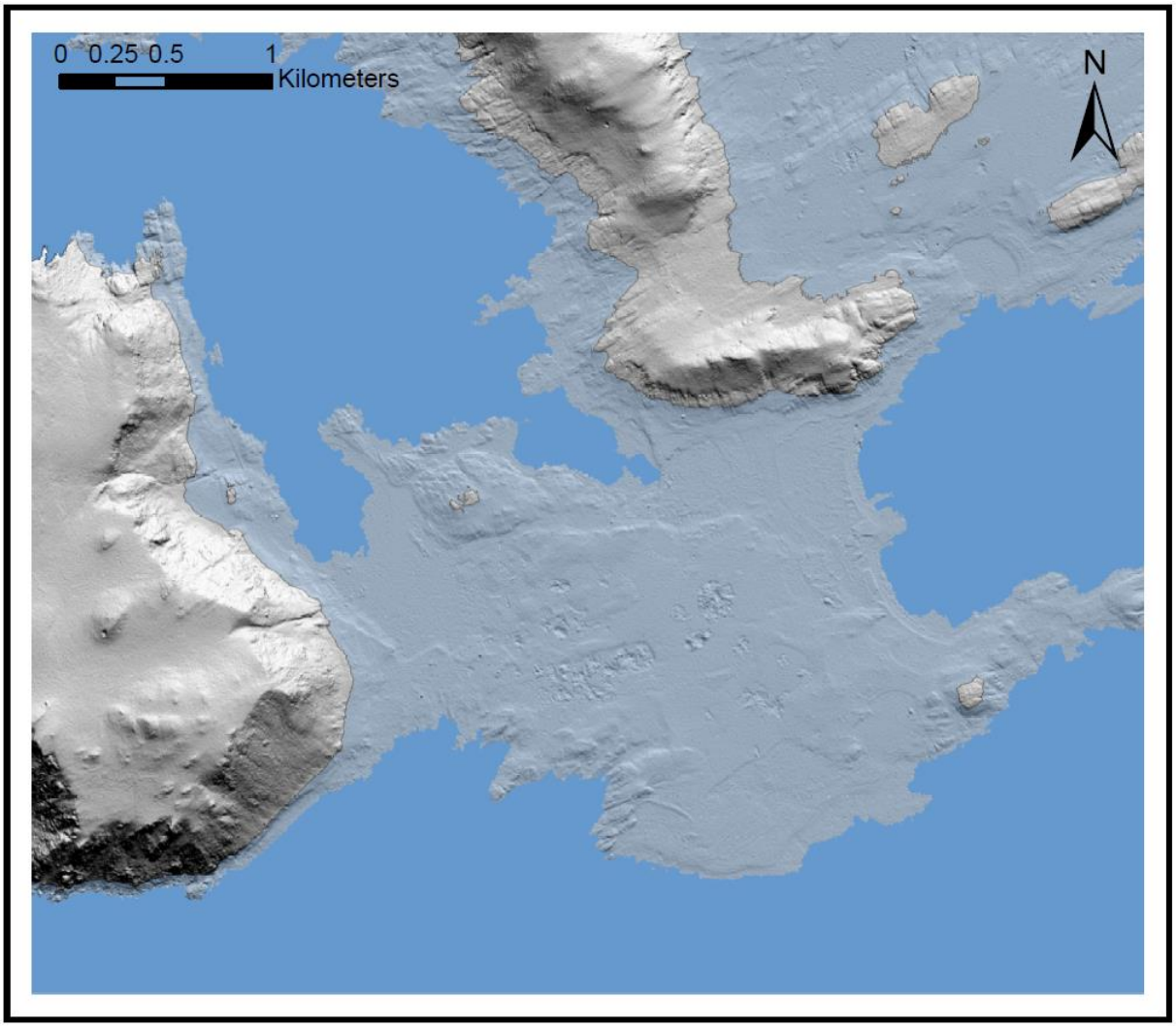

Figure 24. *Marine limit sea level projection on Ingøya.*

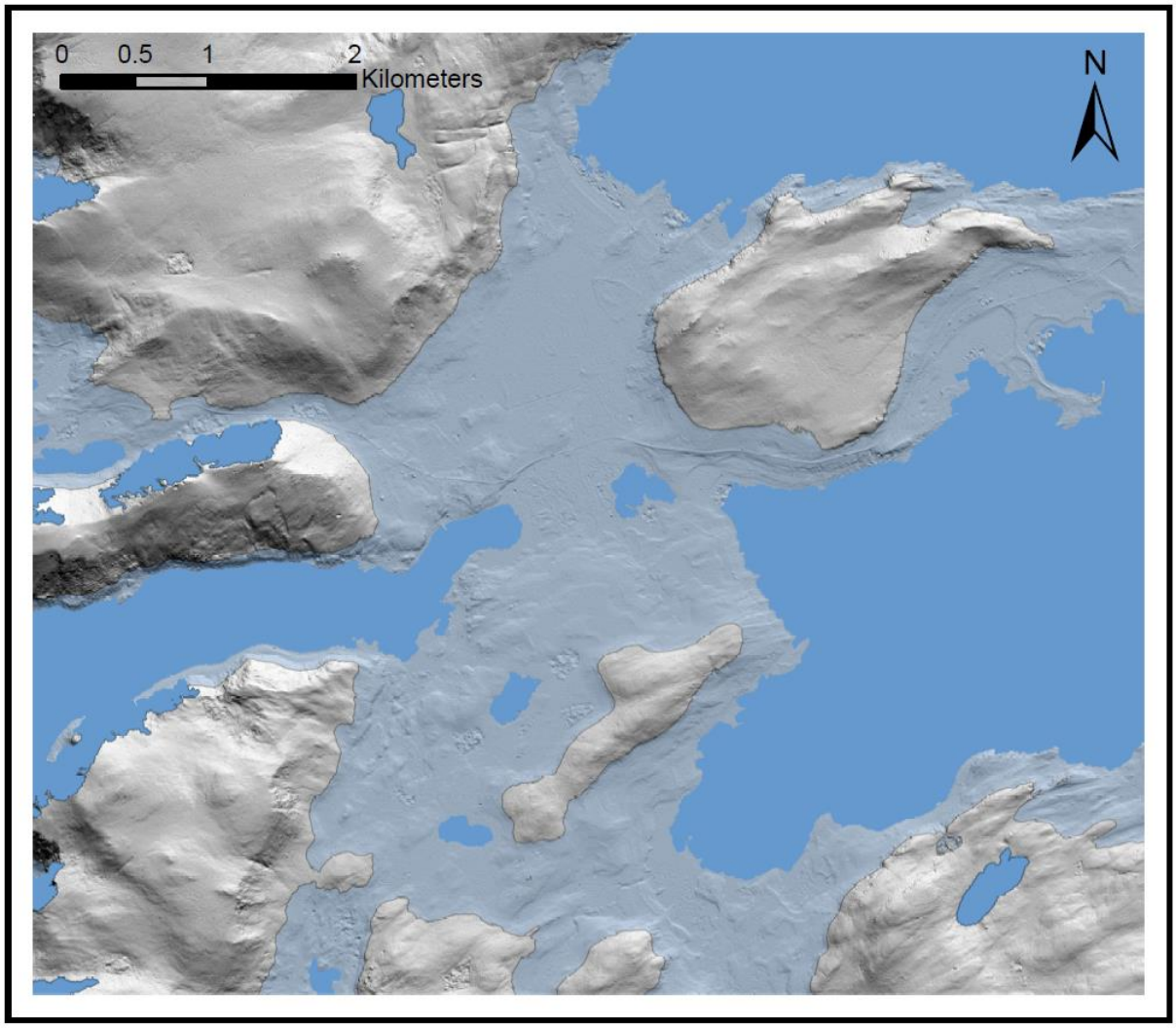

Figure 25. *Marine limit sea level projection on Rolvsøya.*

4.2.2. The Main shoreline and early Holocene low stand – ca. 12 to 8.3 ka

Coincident with the YD readvance, the Main shoreline is noted as a prominent shoreline throughout northern Norway (Sollid et al., 1973). By associating the isolation events at ca. 11 ka on Rolvsøya with this time period, the Main shoreline would have been approximately at 6 m asl. If this is taken to be the elevation of the Main shoreline on both Rolvsøya and Ingøya, then YD beach deposits must be overlain by the postglacial shorelines deposited during late Holocene. From the fjord heads to southern Rolvsøya 100 km to the north, Marthinussen's (1960) Main shoreline 10 ka isobase map suggests Main shoreline elevations ranging from 60 – 10 m. On Ingøya, it is estimated that the Main shoreline isobase is at 0 m. Elsewhere in Norway the YD is marked by a period of relative sea level rise as glacioisostatic rebound slowed with the readvance of the SIS while the global volume of the ocean continued to increase (Wohlfarth et al., 2008).

At the onset of the Holocene, relative sea level fell rapidly as glacial retreat resumed. The early Holocene low stand in sea level following the initial isolation of the 5.23 m asl lakes on Rolvsøya remains unconstrained (Romundset et al., 2011). It is possible that sea level dropped close to or below modern day sea level. Due to the ice margin position approximately 150 km inland at this time, it could be the case that Ingøya and Rolvsøya were relatively uplifted due to the crustal forebulge from isostatic loading of the SIS in central Scandinavia – bringing sea level to its low stand at this time (Andrews, 1974). In Maine, the relative low stand in sea level at -55 m following deglaciation is attributed to this same impact (Barnhardt et al., 1995). The subsequent collapse of the hypothesized glacial forebulge would provide an additional source for sea level rise during the Tapes Transgression. However, early modeling studies due not predict the forebulge to occur on Ingøya (Fjeldskaar, 1994). Determining the source of the Tapes Transgression remains one of the unanswered questions of Norway's relative sea level history.

4.2.3. Storegga tsunami deposit on Ingøya – 8.3 to 8.1 ka

The 8.2 ka submarine Storegga slide off of the continental shelf of western Norway is recorded as the largest gravity mass movement in the world (De Blasio et al., 2005). Most likely triggered by a strong earthquake from the Ormen Lange gas field in the same region, the volume of the Storegga slide was 3100 km^3 with a runout of 400 km (Bryn et al., 2005; De Blasio et al., 2005). The mass movement of the Storegga slide triggered the Storegga tsunami. Lake sediments throughout coastal Norway and the adjacent Shetland islands record this event in the form of graded beds, rip-up clasts, and erosional unconformities (Romundset and Bondevik, 2011; Wohlfarth et al., 2008). Tsunami run-up, measured relative to sea level at 8.2 ka, is recorded to be 11 m in proximal locations to the slide and less than 5 m in areas to the north and south (Bondevik et al., 1997). On Rolvsøya, the run-up of the Storegga Tsunami was determined to be 3 – 5 m relative to sea level at 8.2 ka (Romundset and Bondevik, 2011).

From Romundset et al.'s (2011) marked ingression of the 5.83 m asl lake on Rolvsøya at ca. 8 ka, relative sea level on Ingøya would have been approximately at 5 m at the time of the Storegga tsunami. Based upon this estimate, it is expected that 6 m isolation basin on Ingøya would record the Storegga tsunami in its sedimentary record. Sediment core radiocarbon dates of 7530 ± 10 cal yr BP and 7590 ± 20 cal yr BP from depths of 106 – 109 cm provide an upper constraint for the coarse gravel in unit 4. Although there are no lower constraining ages, the distinct shift between unit 4 and the marine sand in unit 5 is likely an erosional unconformity. On Rolvsøya, sediment cores from 5 m asl lakes contain similar erosional unconformities that are attributed to Storegga tsunami (Romundset and Bondevik, 2011). Attributing the coarse deposit and the erosional unconformity in Ingøya core 23.1 to the Storegga tsunami suggests that all lacustrine sediment deposited during the early Holocene low stand in sea level must have eroded away.

The possibility of lacustrine sediment below the basal marine sand of unit 5 remains due to the lack of age constraints at depth – but this possibility is inconsistent with this identification of the overlying units and the interpretations of their ages. If instead this both the gravel in unit 4 and the sand in unit 5 were attributed to the Tapes, then the corresponding ages of ca. 7500 cal yr BP (n=3) and 5200 cal yr BP (n=2) would be representative of woody macrofossils washed into the basin thousands of years after their death. This interpretation is unlikely, due to the repetition of ages in different fragments from the same depth. Making use of the available information, unit 4 is attributed to the Storegga tsunami.

Identifying unit 4 to be a deposit of the Storegga tsunami provides a constraining age of 8.2 ka to 112 cm. Figure 26 illustrates the isolation basin sedimentary record and sea level at the time of the Storegga tsunami. This identification provides further insight into the relative sea level history of Ingøya. That is, at 8.2 ka sea level must have been somewhere between 1 – 3 m asl, or equivalently, 3 – 5m below the threshold of the 6 m basin.

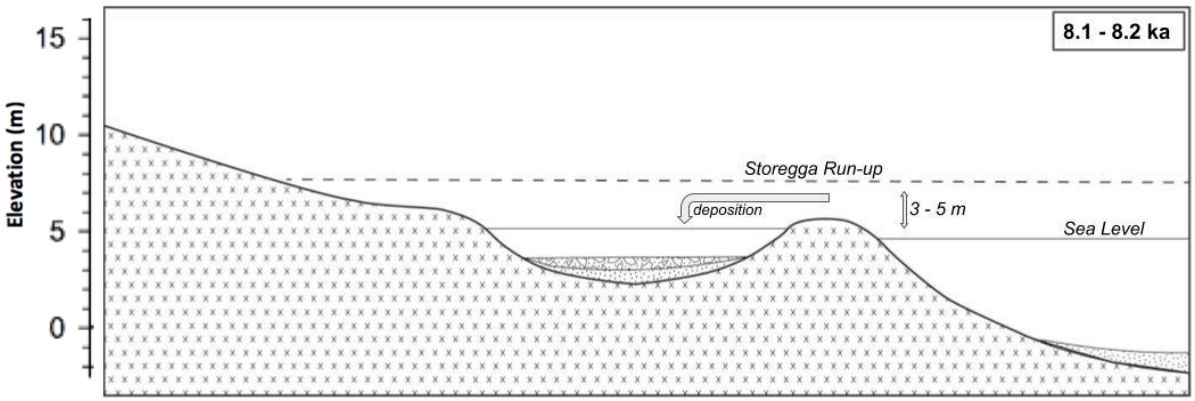

Figure 26. *Schematic cross section of the 6 m asl isolation basin with 3 – 5 m of run-up from the Storegga tsunami, depositing the coarse gravel unit and eroding away the lacustrine unit above the marine sand that would have been deposited during 10 – 8.2 ka.*

4.2.4. Tapes Transgression and post glacial shorelines – 8 to 0 ka

The Tapes Transgression is recorded on Ingøya and Rolvsøya through isolation basin sedimentary records, a transgressive bench-like terrace that marks the height of the transgression on south-central Ingøya (Retelle, unpublished), as well as a gravelly spit-like landform with shells and drift pumice on northeastern Rolvsøya. The timing of the Tapes Transgression is constrained by ages of 8 – 5 ka obtained from isolation basins on Rolvsøya and elsewhere in Finnmark, both to the south on Sørøya and to the east the Nordkinn Peninsula (Romundset et al., 2011). Specifically, the rise and fall of sea level during Tapes Transgression in the mid Holocene is recorded through inundation and isolation events in basins up to 5 m asl. In southern Norway, the timing of the Tapes Transgression is similarly constrained to 5 – 8 ka and marked by deposits of olive-brown to olive-grey gytia containing small amounts of silt and fine sand (Bondevik et al., 1998). On Ingøya, sediment core radiocarbon ages of ca. 7500 cal yr BP (n=3) and ca. 5200 cal yr BP (n=2) reflect a similar timing to the Tapes Transgression. However, it is necessary to identify the sedimentary unit that they constrain as one of marine origin in order to relate them as inundation and isolation events.

Although the $\delta^{13}C$ and C/N signature of sediment in unit 2 indicates a terrestrial origin, it is highly unlikely that the basin was entirely a lacustrine environment throughout this period. The height of Tapes Transgression on Ingøya (9 m asl) and Rolvsøya (9.8 m asl) is dated to ca. 6,200 cal yr BP from bivalves from the uppermost Tapes shoreline (Retelle, unpublished). This result indicates that the 6 m asl basin must have been inundated during a portion of the Tapes Transgression. Considering the downcore profiles of Fe, $\delta^{13}C$, and C/N together, a synchronous shift at 65 cm indicates a changing environment within the basin. The profiles of $\delta^{13}C$ and C/N signal a terrestrial source of sedimentary organic, with values of -28‰ and 22 respectively (Lamb et al., 2006). A sudden decrease in Fe at 65 cm moving up core is indicative of changing

basin conditions and consistent with the absence of oxidized sediment in this same unit. The presence of oxidized sediment and fine sand and micas throughout unit 2 may be representative of a low energy marine embayment.

Despite the absence of foraminifera in unit 2, the eelgrass *Zostera marina was* identified. However, the δ^{13}C value of -26‰ from 2.12 µmol of *Zostera marina* sample does not align with the -9 – -12‰ range that is typically indicative of this species. Contrary to this, the %C value 30.38% is in agreement with previous analysis of *Zostera marina* in the Bates College Environmental Geochemistry Laboratory. It is possible insufficient cleaning of other organic matter in the sediment ultimately gave the fragments a more depleted δ^{13}C signature. It could also be the case that lower temperatures in this high latitude environment resulted in preferential fractionation of the lighter ^{12}C isotope upon diffusion of CO_2 into the water column from the atmosphere (Sharp, 2017). Additionally, the diffusion of less ^{13}C from C3 plants in the sediment could cause for depleted δ^{13}C values in the water. If both of these effects depleted the δ^{13}C of the water, it would be expected that the δ^{13}C signature of *Zostera marina* would be depleted as well. Based upon this reasoning and visual appearance, these fragments are taken to be *Zostera marina*, a marine species whose presence helps support the marine origin of unit 2. Additionally, numerous chironomid head capsules were also found at this depth. Chironomids are known to thrive in lacustrine environments while at the same time being capable of living in brackish and intertidal environments (Pinder, 1995). This evidence supports the height of the Tapes Transgression at 9 m asl. The isolation basin environments on Ingøya from the height of the Tapes Transgression to modern day are depicted in Figure 27.

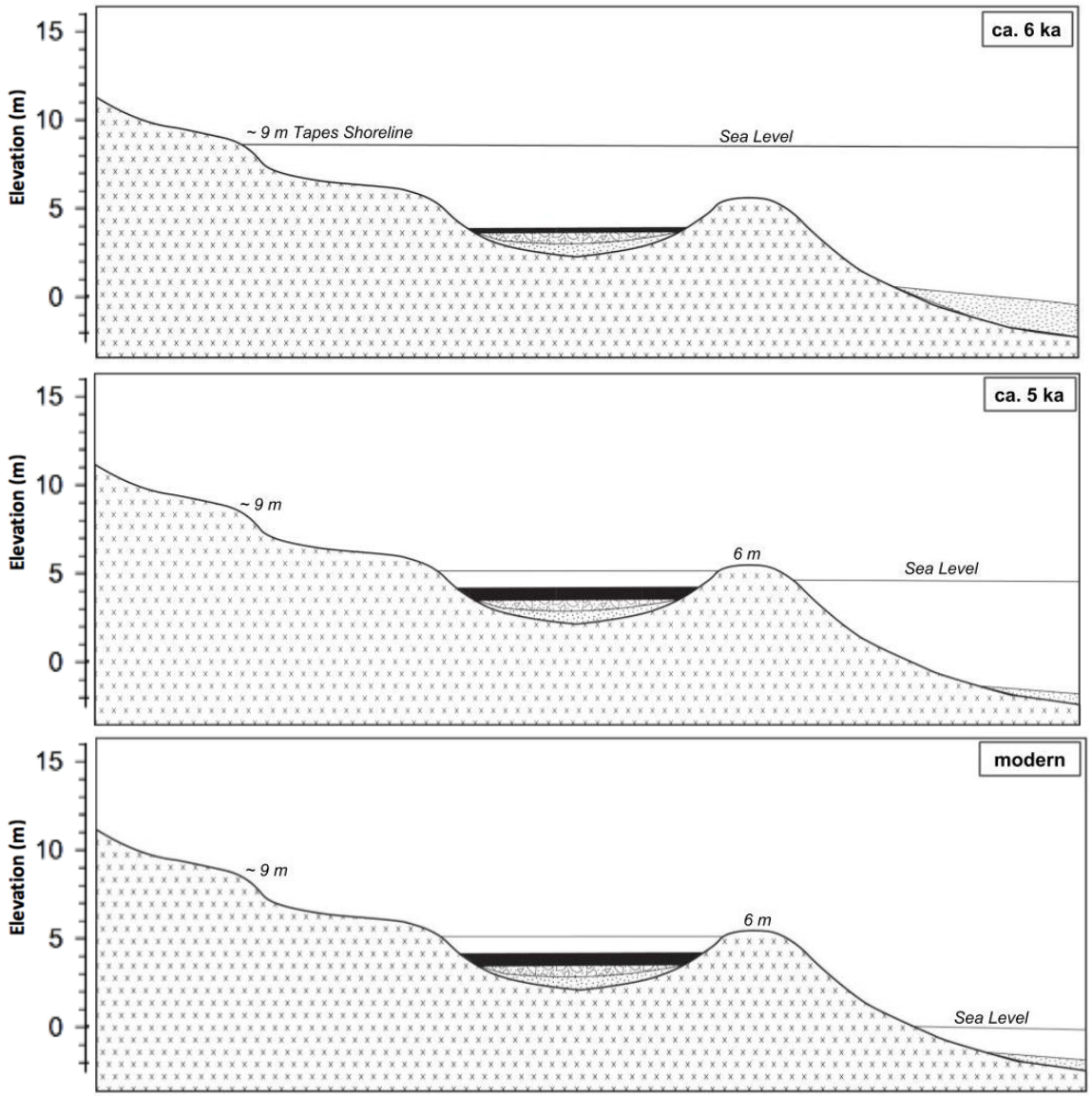

Figure 27. *Time transgressive sequence of isolation basin sedimentation from the height of Tapes (top) to the isolation event (middle) to the present day (bottom).*

The recorded height of the Tapes Transgression on Ingøya and Rolvsøya from this study conflicts with previous relative sea level reconstructions and models for this region (Jakob et al., 1989; Romundset et al., 2011; Snyder et al., 1996). Both Jakob et al. (1989) and Snyder et al. (1996) present 6 ka isobase maps positioning the 5 m isobase on Ingøya and Rolvsøya. This is reflected in Romundset et al.'s (2011) reconstruction on Rolvsøya. However, numerous ca. 6,200 cal yr BP dated marine bivalves found in situ on the uppermost Tapes Shoreline reject these previous reconstructions. Relative sea level reconstruction on Sørøya and the Nordkinn Peninsula place the height of the Tapes Transgression at 10 m asl and 11 m asl, respectively,

consistent with the dated Tapes shoreline on Rolvsøya and Ingøya (Romundset et al., 2011). A 6 ka isobase map based on the elevation of these shorelines across northern Finnmark illustrates crustal response since the mid Holocene (Figure 28). Far to the east on the Kola Peninsula, the Tapes Transgression reached a height of 11 – 16 m asl (Snyder et al., 1996). Projecting sea level on the ArcticDEM at the height of the Tapes Transgression with correction for isostatic tilt shows the position shorelines would occur at around 6.2 ka (Figures 29 - 31).

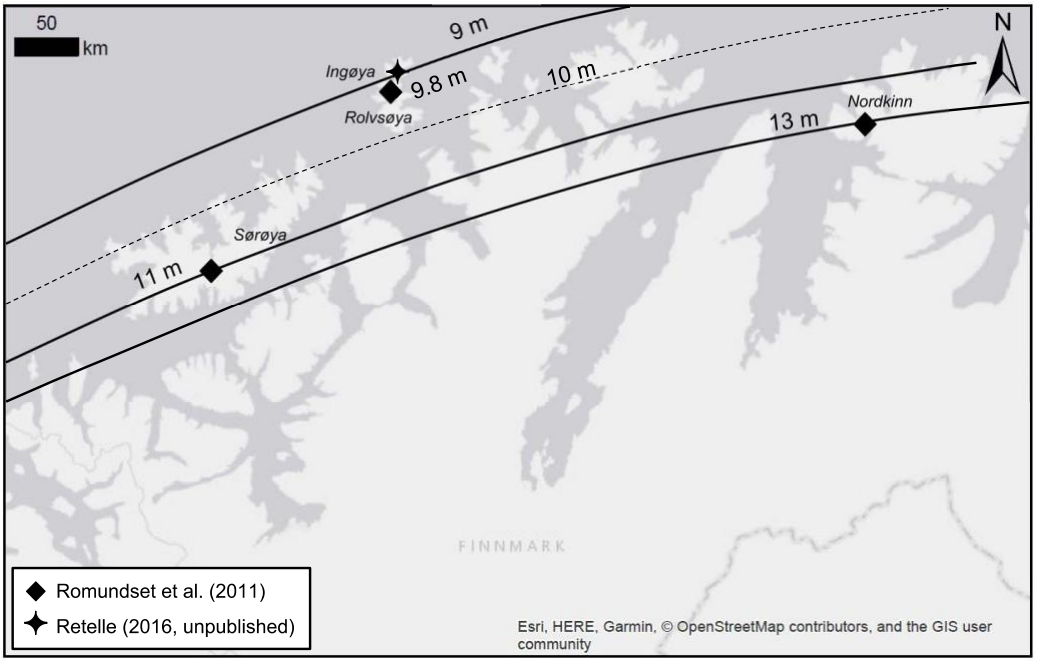

Figure 28. *6 ka isobase based on the height of the Tapes from Retelle (2016) and Romundset et al. (2011).*

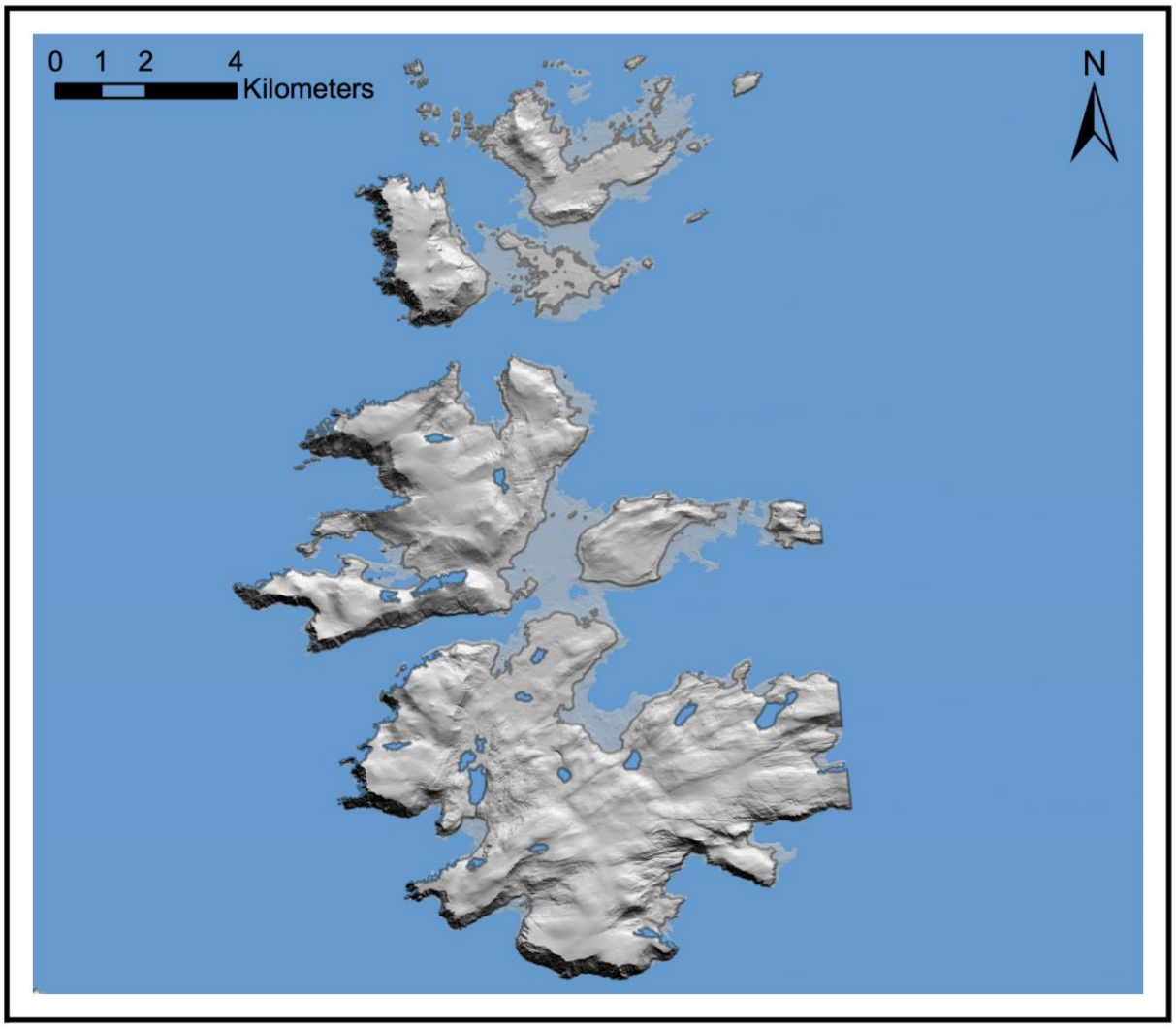

Figure 29. *Tapes Shoreline projection with a 0.2 m km^{-1} tilt correction from north to south. Notice, with this projection the isolation basin considered in this study, as well as the basins in Romundset et al. (2011), are inundated.*

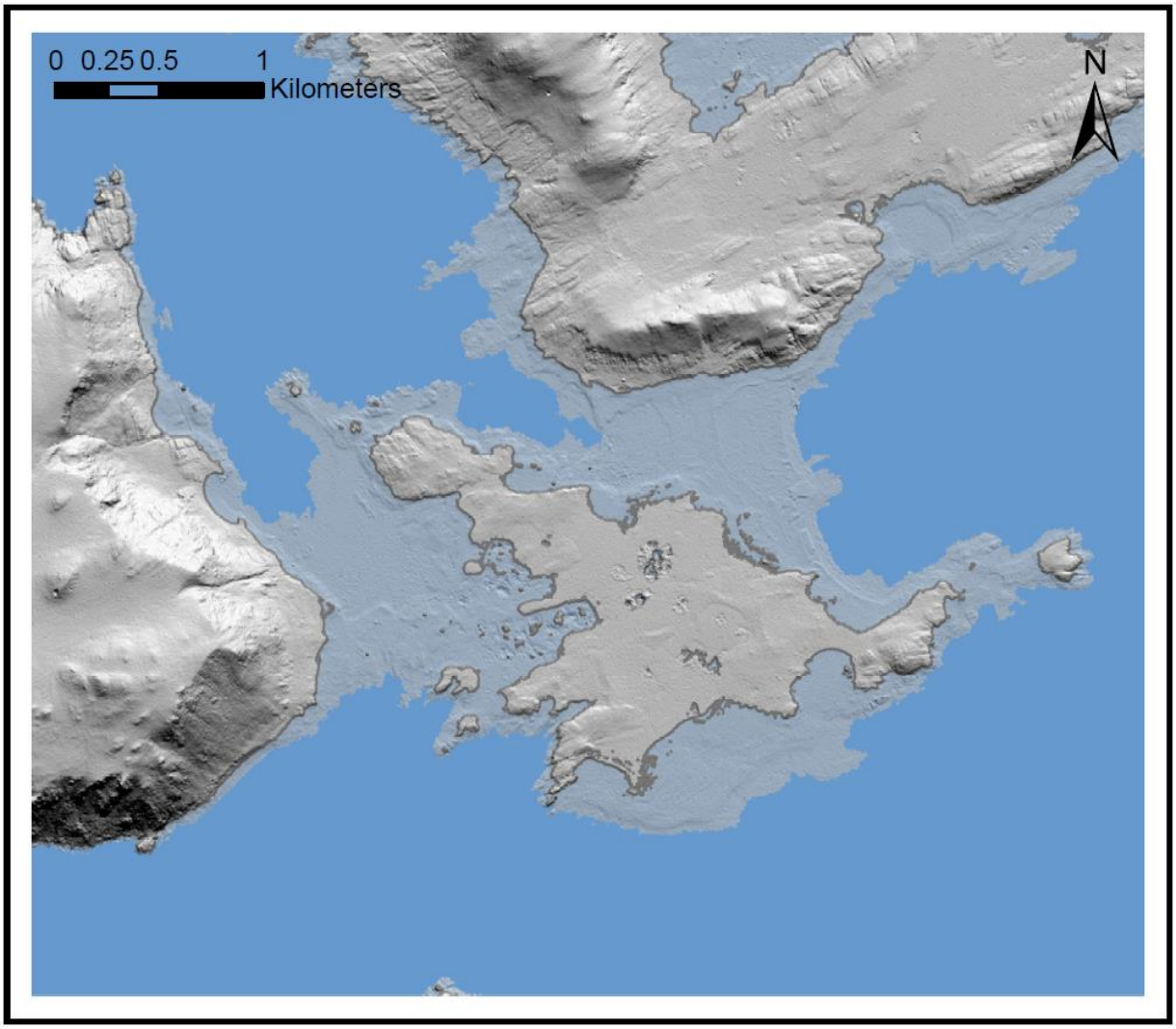

Figure 30. *Tapes Shoreline projection on southern Ingøya.*

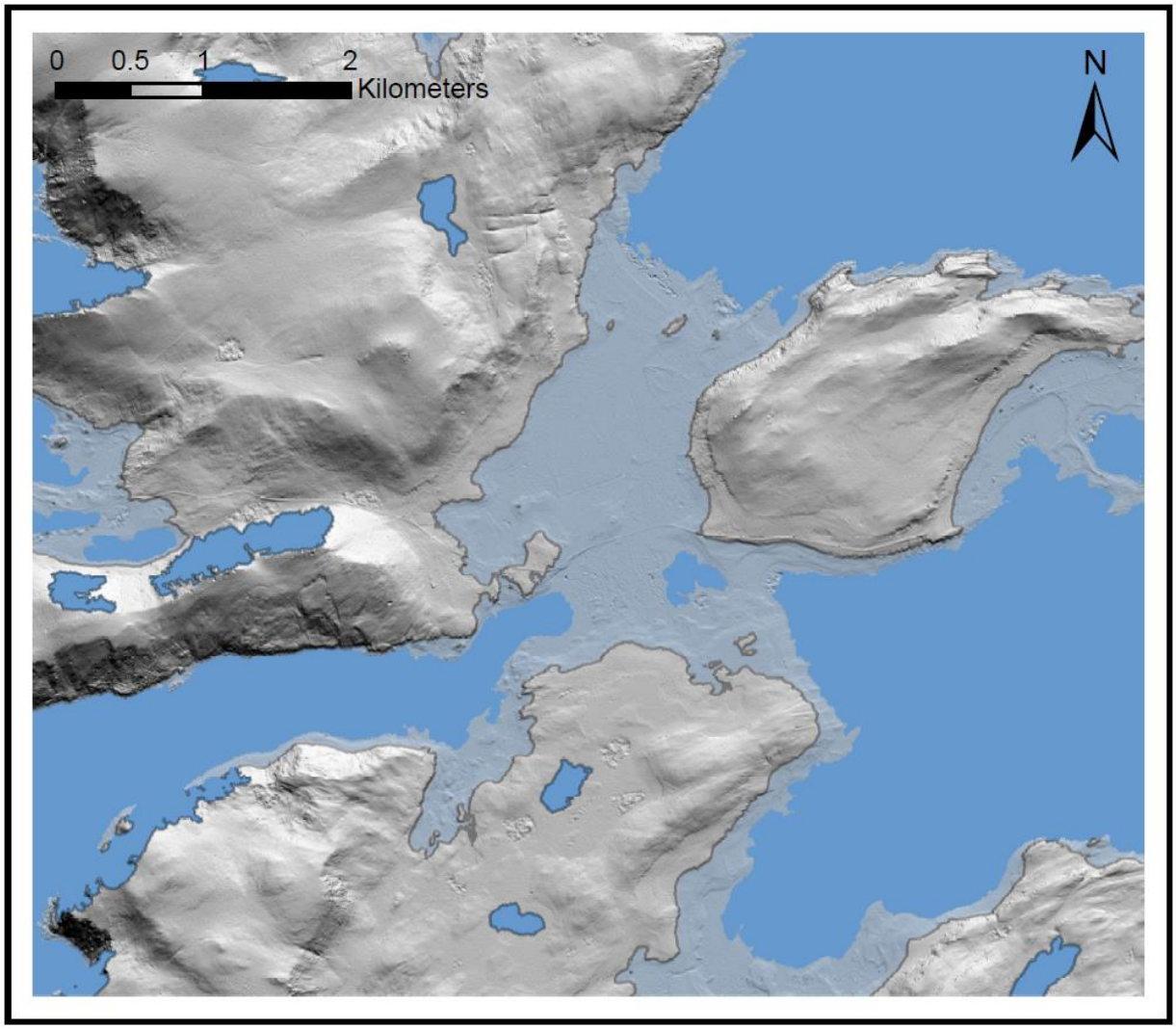

Figure 31. *Tapes Shoreline projection on central Rolvsøya*

Regression from the Tapes Shoreline resulted in a flight of late Holocene beaches containing bivalves and drift pumice. The occurrence of drift pumice at the highest Tapes Shoreline is consistent with the history of volcanism in Iceland and field observations throughout Norway (Binns, 1972). Radiocarbon dates on bivalves are interpreted as the maximum elevation for sea level throughout the late Holocene, since it is possible for an older shell to be transported to a higher shoreline during a storm. Gravel storm ridges are known to occur several meters above the high tide mark in wave dominated environments (Otvos, 2000). Although these shells were taken from a lower energy sandy shoreline, the measured height of the shoreline is considered to be above the high tide mark for that time period. Hence, these ages on marine bivalves represent a maximum elevation for sea level. As a result, the late Holocene relative sea level history is well defined on both Rolvsøya and Ingøya (Retelle, unpublished).

5. Conclusion

Dating of both the marine limit 30 m asl shoreline and the 20 m asl late glacial shoreline on Ingøya through cosmogenic ^{10}Be further defines the relative sea level history of this region. Sediment core radiocarbon ages from the Ingøya isolation basin further constrain the timing of the Tapes Transgression and indicate previously obtained ages of marine bivalves provide a maximum elevation of relative sea level during the mid-Holocene. The main findings from this study are:

1. Deglaciation of the north coast of Finnmark at ca. 14.8 ka, as defined by ^{10}Be ages in agreement with the regional chronology of deglaciation.
2. Rapid postglacial isostatic uplift of the region prior to the Holocene.
3. Inundation on Ingøya at 6 m asl from the 8.2 ka Storegga Tsunami.
4. Further agreement of the timing of the 8 – 5 ka Tapes Transgression through ^{14}C AMS ages on woody plant macrofossils of 7590 ± 20 cal yr BP and 5318 ± 5 cal yr BP.

The addition of this work to the body of literature surrounding postglacial sea level can refine our understanding of the spatial variability of eustatic and isostatic processes. Variability in the elevation of late-glacial shoreline provides a basis for reconstructing patterns of isostatic loading. Additionally, few sea level reconstructions have utilized cosmogenic nuclides to date raised shorelines and this work supports the utility of this technique in locations that lack dateable organic material. More importantly, the nature of rapid sea level rise through eustatic changes (and possibly isostatic adjustments) can be explored through understanding the Tapes Transgression. Better constraining rates of change during this transgressive period is important when considering the analogous modern day situation. How does the remaining decay of ice sheets during the mid-Holocene alter sea level on Ingøya? Do these changes mirror the current and anticipated sea level rise due to the melting of Greenland and Antarctica in the 21st century? To better answer these questions more work is necessary.

The relative sea level history for the outer north coast of Norway is poorly constrained from the early Holocene to the onset of the Tapes Transgression. Exploration of basins at or below sea level would give a better control for the early Holocene low stand in sea level. A sediment core from a low energy, modern day marine basin at low tide could provide the necessary evidence. Possible locations exist on central Ingøya, either near the Molo (Savage, 2016) or inner Mafjorden. Additionally, more surface exposure dates of marine limit shorelines would provide better spatial control for deglaciation. Cosmogenic surface exposure dates from marine limit shorelines at any of Romundset et al.'s (2011) study locations would provide more dates of deglaciation while complementing existing relative sea level curves. To answer the larger, process oriented questions – i.e. what is the source for the Tapes Transgression – it would be useful to consider the sea level history along a north-south transect in this region

while focusing on the nature of sea level rise at this time. The importance of understanding these dynamics and processes in greater detail is underscored when considering rising sea levels around the world today.

References

Andersen, B., 1965, Glacial chronology of Western Troms, North Norway: GSA, v. 84, p. 35-54.

Andrews, J., 1974, Glacial Systems: an approach to glaciers and their environments, North Scituate, Massachusetts, Duxbury Press.

Balco, G., Briner, J., Finkel, R. C., Rayburn, J. A., Ridge, J. C., and Schaefer, J. M., 2009, Regional beryllium-10 production rate calibration for late-glacial northeastern North America: Quaternary Geochronology, v. 4, no. 2, p. 93-107.

Balco, G., Stone, J. O., Lifton, N. A., and Dunai, T. J., 2008, A complete and easily accessible means of calculating surface exposure ages or erosion rates from 10Be and 26Al measurements: Quaternary Geochronology, v. 3, no. 3, p. 174-195.

Barber, D., Dyke, A., Hillaire-Marcel, C., Jennings, A., Andrews, J., W. Kerwin, M., Bilodeau, G., McNeely, R., Southon, J., Morehead, M., and Gagnon, J.-M., 1999, Forcing of the cold event of 8,200 years ago by catastrophic drainage of Laurentide lakes, 344-348 p.:

Barnhardt, W., Gehrels, W., Belknap, D., and Kelley, J., 1995, Late Quaternary relative sea-level change in the wester Gulf of Maine: Evidence for a migrating glacial forebulge: Geology, v. 23, p. 317-320.

Bergstrøm, B., Olsen, L., and Sveian, H., 2005, The Tromsø-Lyngen glacier readvance (early Younger Dryas) at Hinnøya-Ofotfjorden, northern Norway: a reassessment: NGU Bulletin, v. 45, p. 73-88.

Bierman, P., Rood, D., Shakun, J., Portenga, E., and Corbett, L., 2016, Directly dating post-glacial Greenlandic emergence at high resolution using in situ 10Be: For submission to Quaternary Research, p. 36.

Binns, R., 1972, Composition and derivation of pumice on postglacial strandlines in northern Europe and the Western Arctic: Geological Society of America Bulletin, v. 83, p. 2303-2324.

Bondevik, S., Svendsen, J., and Mangerud, J., 1998, Distinction between the Storegga tsunami and the Holocene marine transgression in coastal basin deposits of western Norway: Journal of Quaterary Science, v. 13, p. 529-537.

Bondevik, S., Svendsen, J. I., Johnsen, G., Mangerud, J., and Kaland, P. E., 1997, The Storegga tsunami along the Norwegian coast, its age and runup: Boreas, v. 26, no. 1, p. 29-53.

Bryn, P., Berg, K., Forsberg, C. F., Solheim, A., and Kvalstad, T. J., 2005, Explaining the Storegga Slide: Marine and Petroleum Geology, v. 22, no. 1, p. 11-19.

Clark, P. U., Dyke, A. S., Shakun, J. D., Carlson, A. E., Clark, J., Wohlfarth, B., Mitrovica, J. X., Hostetler, S. W., and McCabe, A. M., 2009, The Last Glacial Maximum: Science, v. 325, no. 5941, p. 710-714.

Corbett, L., Bierman, P., and Rood, D., 2016, An approach for optimizing in *situ* cosmogenic 10Be sample preparation: Quaternary Geochronology, v. 33, p. 24-34.

Corfu, F., Roberts, R., Torsvik, T., Ashwal, L., and Ramsay, D., 2007, Peri-Gondwanan elements in the Caledonian nappes of Finnmark, northern Norway: implications for the paleogeographic framework of the Scandinavian Caledonides: American Journal of Science, v. 307, p. 434-458.

Croudace, I., and Rothwell, R., 2015, Micro-XRF Studies of Sediment Cores, Springer, 668 p.:

De Blasio, F. V., Elverhøi, A., Issler, D., Harbitz, C. B., Bryn, P., and Lien, R., 2005, On the dynamics of subaqueous clay rich gravity mass flows—the giant Storegga slide, Norway: Marine and Petroleum Geology, v. 22, no. 1, p. 179-186.

Evans, D., Rea, B., Hansom, J., and Whalley, W., 2002, Geomorphology and style of plateau icefield deglaciation in fjord terrains: the example of Troms-Finnmark, north Norway: Journal of Quaterary Science, v. 17, p. 221-239.

Fenton, C. R., Hermanns, R. L., Blikra, L. H., Kubik, P. W., Bryant, C., Niedermann, S., Meixner, A., and Goethals, M. M., 2011, Regional 10Be production rate calibration for the past 12ka deduced from the radiocarbon-dated Grøtlandsura and Russenes rock avalanches at 69° N, Norway: Quaternary Geochronology, v. 6, no. 5, p. 437-452.

Fjeldskaar, W., 1994, The amplitude and decay of the glacial forebulge in Fennoscandia: Norsk Geologisk Tidsskrift, v. 74, p. 2-8.

Hellborg, R., and Skog, G., 2008, Accelerator mass spectrometry: Mass Spectrometry Reviews, v. 27, no. 5, p. 398-427.

Hughes, A., Gyllenceutz, R., Lohne, Ø., Mangerud, J., and Svendsen, J., 2016, The last Eurasian ice sheets - a chronological database and time-slice reconstruction, DATED-1: Boreas, v. 45, no. 1-45.

Ingólfsson, Ó., and Hjort, C., 1999, The Antarctic contribution to Holocene global sea level rise: Polar Research, v. 18, no. 2, p. 323-330.

Ivy-Ochs, S., and Kober, F., 2008, Surface exposure dating with cosmogenic nuclides: Quaternary Science Journal, v. 57, p. 179-209.

Jakob, J. M., xf, and ller, 1989, Geometric Simulation and Mapping of Holocene Relative Sea-Level Changes in Northern Norway: Journal of Coastal Research, v. 5, no. 3, p. 403-417.

Jane, S., John, G., Rick, T., Bob, O., James, F., and V., J. J., 2007, Atmospheric scaling of cosmogenic nuclide production: Climate effect: Journal of Geophysical Research: Solid Earth, v. 112, no. B2.

Lamb, A. L., Wilson, G. P., and Leng, M. J., 2006, A review of coastal palaeoclimate and relative sea-level reconstructions using δ13C and C/N ratios in organic material: Earth-Science Reviews, v. 75, no. 1, p. 29-57.

Lambeck, K., and Chappell, J., 2001, Sea level change through the last glacial cycle: Science, v. 292, no. 5517, p. 679-686.

Landvik, J. Y., Bondevik, S., ElverhØI, A., Fjeldskaar, W., Mangerud, J. A. N., Salvigsen, O., Siegert, M. J., Svendsen, J.-I., and Vorren, T. O., 1998, THE LAST GLACIAL MAXIMUM OF SVALBARD AND THE BARENTS SEA AREA: ICE SHEET EXTENT AND CONFIGURATION: Quaternary Science Reviews, v. 17, no. 1, p. 43-75.

Larsen, E., Fredin, O., Lysa, A., Amantov, A., Fjeldskaar, W., and Ottesen, D., 2016, Causes of time-transgressive glacial maxima positions of the last Scandinavian Ice Sheet: Norwegian Journal of Geology, v. 96, p. 159-170.

Long, A. J., Woodroffe, S. A., Roberts, D. H., and Dawson, S., 2011, Isolation basins, sea-level changes and the Holocene history of the Greenland Ice Sheet: Quaternary Science Reviews, v. 30, no. 27, p. 3748-3768.

Mangerud, J., 1972, Radiocarbon dating of marine shells, including a discussion of apparent age of Recent shells from Norway, Boreas.

Mangerud, J., 2004, Ice sheet limits on Norway and the Norwegian continental shelf.

Mangerud, J., Gyllenceutz, R., Lohne, Ø., and Svendsen, J., 2011, Glacial History of Norway: Developments in Quaternary Science.

Mangerud, J. A. N., Gulliksen, S., Larsen, E., Longva, O., Miller, G. H., Sejrup, H.-P., and SØNstegaard, E., 1981, A Middle Weichselain ice-free period in Western Norway: the Ålesund Interstadial: Boreas, v. 10, no. 4, p. 447-462.

Mark, S., 2016, Mid-Holocene Marine Paleoclimate Reconstruction Through Schlerochronological Analysis of Arctica islandica from Finnmark, Rolvsøya, Northern Norway, 154 p.

Marthinussen, M., 1962, C14 datings referring to shore lines, transgressions, and glacial substages in Northern Norway, Norges geologiske.

Nishiizumi, K., Imamura, M., Caffee, M. W., Southon, J. R., Finkel, R. C., and McAninch, J., 2007, Absolute calibration of 10Be AMS standards Nuclear Instruments and Methods in Physics Research v. v. 259, p. p. 403–413.

Ottensen, D., Stokes, C., Rise, L., and Olsen, L., 2008, Ice-sheet dynamics and ice streaming along the coastal parts of northern Norway: Quaternary Science Reviews, v. 27, p. 922-940.

Otvos, E. G., 2000, Beach ridges — definitions and significance: Geomorphology, v. 32, no. 1, p. 83-108.

Peltier, W. R., 1998, Postglacial variations in the level of the sea: Implications for climate dynamics and solid-earth geophysics: Reviews of Geophysics, v. 36, no. 4, p. 603-689.

Piasecka, E., Winsborrow, M., Andreassen, K., and Stokes, C., 2016, Reconstructing the retreat dynamics of the Bjørnøyrenna Ice Stream based on new 3D seismic data from the central Barents Sea: Quaternary Science Reviews, v. 151, p. 212-227.

Pinder, 1995 The habitats of chironomid larvae The Chironomidae: Dordrecht, Springer.

Reimer, P. J., Bard, E., Bayliss, A., Beck, J. W., Blackwell, P. G., Bronk Ramsey, C., Buck, C. E., Cheng, H., Edwards, R. L., Friedrich, M., Grootes, P. M., Guilderson, T. P., Haflidason, H., Hajdas, I., Hatté, C., Heaton, T. J., Hoffmann, D. L., Hogg, A. G., Hughen, K. A., Kaiser, K. F., Kromer, B., Manning, S. W., Niu, M., Reimer, R. W., Richards, D. A., Scott, E. M., Southon, J. R., Staff, R. A., Turney, C. S. M., and van der Plicht, J., 2013, IntCal13 and Marine13 radiocarbon age calibration curves 0-50,000 years cal BP: Radiocarbon, v. 55, no. 4, p. 1869-1887.

Renssen, H., Seppä, H., Crosta, X., Goosse, H., and Roche, D. M., 2012, Global characterization of the Holocene Thermal Maximum: Quaternary Science Reviews, v. 48, no. Supplement C, p. 7-19.

Riva, R. E. M., Bamber, J. L., Lavallée, D. A., and Wouters, B., 2010, Sea-level fingerprint of continental water and ice mass change from GRACE: Geophysical Research Letters, v. 37, no. 19.

Romundset, A., Akcar, N., Fredin, O., Titkhomirov, D., Reber, R., Vockenhuber, C., Christl, M., and Schlüchter, C., 2017, Lateglacial retreat chronology of the Scandinavian Ice Sheet in Finnmark, northern Norway, reconstructed from surface exposure dating of major end moraines: Quaternary Science Reviews, v. 177, p. 120-144.

Romundset, A., and Bondevik, S., 2011, Propagation of the Storegga tsunami into ice-free lakes along the southern shores of the Barents Sea: Journal of Quaternary Science, v. 26, no. 5, p. 457-462.

Romundset, A., Bondevik, S., and Bennike, O., 2011, Postglacial uplift and relative sea level changes in Finnmark, northern Norway: Quaternary Science Reviews, v. 30, p. 2398-2421.

Savage, J., 2016, A Late-Holocene Marine Climate Reconstruction Using the Bivalve Arctica islandica from Northern Norway, 153 p.

Sejrup, H. P., Nygård, A., Hall, A. M., and Haflidason, H., 2009, Middle and Late Weichselian (Devensian) glaciation history of south-western Norway, North Sea and eastern UK: Quaternary Science Reviews, v. 28, no. 3, p. 370-380.

Sharp, Z., 2017, Principles of Stable Isotope Geochemistry, 2nd Edition.

Snyder, J. A., Korsun, S. A., and Forman, S. L., 1996, Postglacial emergence and the Tapes transgression, north-central Kola Peninsula, Russia: Boreas, v. 25, no. 1, p. 47-56.

Sollid, J., Andersen, S., Hamre, N., Kjeldsen, O., Salvigsen, O., Strurod, S., Tveita, T., and Wilhelmsen, A., 1973, Deglaciation of Finnmark, North Norway, Norsk geogr, Tidsskr.

Stroeven, A. P., Hättestrand, C., Kleman, J., Heyman, J., Fabel, D., Fredin, O., Goodfellow, B. W., Harbor, J. M., Jansen, J. D., Olsen, L., Caffee, M. W., Fink, D., Lundqvist, J., Rosqvist, G. C., Strömberg, B., and Jansson, K. N., 2016, Deglaciation of Fennoscandia: Quaternary Science Reviews, v. 147, p. 91-121.

Sturt, B., Pringle, I., and Roberts, D., 1975, Caledonian Nappe Sequence of Finnmark, Northern Norway, and the Timing of Orogenic Deformation and Metamorphism: Geological Society of America Bulletin, v. 86, p. 710-718.

Synge, F., 1969, The raised shorelines and deglaciation chronology of Inari, Finland, and South Varanger, Norway, Physical Geography.

Winsborrow, M., Andreassen, K., Corner, G., and Laberg, J., 2010, Deglaciation of a marine-based ice sheet: Late Weichselian palaeo-ice dynamics and retreat in the southern Barents Sea reconstructed from onshore and offshore glacial geomorphology: Quaternary Science Reviews, v. 29, p. 424-442.

Wohlfarth, B., Björck, S., Funder, S., Houmark-Nielsen, M., Ingólfsson, Ó., Lunkka, J. P., Mangerud, J., Saarnisto, M., and Vorren, T. O., 2008, Quaternary of Norden: Episodes, v. 31, no. 1, p. 73-81.

Appendix A: PRIME ^{10}Be data

Sample Name	Quartz Mass (g)	Mass of ^{9}Be Added (µg)*	AMS Cathode Number	Uncorrected ^{10}Be/^{9}Be Ratio**	Uncorrected ^{10}Be/^{9}Be Ratio unc.**	Background Corrected ^{10}Be/^{9}Be Ratio	Background Corrected ^{10}Be/^{9}Be Ratio unc.	^{10}Be conc. (atoms/g)	10Be conc. unc. (atoms/g)
C1	21.4018	0.8400	147100	1.060×10^{-13}	4.312×10^{-15}	1.054×10^{-13}	4.340×10^{-15}	7.952×10^{4}	3.273×10^{3}
C2	21.0847	0.8413	147101	8.557×10^{-14}	3.298×10^{-15}	8.499×10^{-14}	3.335×10^{-15}	6.516×10^{4}	2.557×10^{3}
C3	21.8772	0.8396	147102	8.418×10^{-14}	3.087×10^{-15}	8.359×10^{-14}	3.126×10^{-15}	6.164×10^{4}	2.305×10^{3}
C4	21.6765	0.8394	147103	8.078×10^{-14}	2.876×10^{-15}	8.019×10^{-14}	2.918×10^{-15}	5.967×10^{4}	2.171×10^{3}
C5	22.1454	0.8380	147104	8.779×10^{-14}	3.070×10^{-15}	8.721×10^{-14}	3.110×10^{-15}	6.341×10^{4}	2.261×10^{3}
C6	21.8734	0.8377	147105	8.559×10^{-14}	3.084×10^{-15}	8.501×10^{-14}	3.123×10^{-15}	6.255×10^{4}	2.298×10^{3}
C7	21.1340	0.8391	147106	8.576×10^{-14}	2.822×10^{-15}	8.517×10^{-14}	2.865×10^{-15}	6.498×10^{4}	2.186×10^{3}
C8	21.5328	0.8377	147107	8.490×10^{-14}	2.948×10^{-15}	8.431×10^{-14}	2.989×10^{-15}	6.302×10^{4}	2.234×10^{3}
C9	21.2592	0.8390	147108	8.614×10^{-14}	3.498×10^{-15}	8.555×10^{-14}	3.532×10^{-15}	6.487×10^{4}	2.679×10^{3}
C10	21.9220	0.8383	147109	9.947×10^{-14}	3.675×10^{-15}	9.888×10^{-14}	3.708×10^{-15}	7.265×10^{4}	2.725×10^{3}

*9Be was added through a beryl carrier made at University of Vermont with a concentration of 291 µg mL-1.

**Isotopic analysis was conducted at PRIME Laboratory; ratios were normalized against standard 07KNSTD3110 with an assumed ratio of 2850 x 10-15 (Nishiizumi et al., 2007).

Appendix A. Laboratory data reduction of the ^{10}Be/^{9}Be ratio derived from the beach cobbles processed quartz to the give the concentration of cosmogenic ^{10}Be produced in situ.

Appendix B: Sediment core stable isotope and geochemistry

Depth (cm)	$\delta^{13}C$	C/N	%C
0	-28.42	26.9	15.54
5	-28.56	19.47	3.9
10	-28.83	21.01	14.21
15	-28.45	19.79	6.57
20	-28.72	19.36	27.76
25	-28.53	19.67	14.63
30	-28.62	23.87	34.25
35	-28.7	27.41	35.79
40	-28.89	21.43	30.82
45	-28.56	21.64	25.49
50	-28.51	23.5	25.85
55	-28.51	24.97	30.97
60	-28.85	21.85	20.31
65	-28.29	18.98	29.01
70	-26.53	18.46	5.78
75	-26.29	18.23	27.17
80	-26.23	17.5	29.54
85	-25.27	17.85	19.07
90	-25.6	19.07	13.68
95	-25.31	15.79	2.66
100	-25.74	18.9	4.36
105	-27.38	22.37	27.91
110	-26.53	19.14	5.21
115	-26.23	9.48	0.21
120	-25.28	10.61	0.1
125	-24.39	8.23	0.07
130	-25.17	11	0.09

Depth (cm)	$\delta^{13}C$	C/N	%C
135	-22.43	5.29	0.06
140	-26.06	10.45	0.27
145	-24.16	9.5	0.11
150	-25.48	11.55	0.18
155	-25.14	13.26	0.08
160	-22.31	10.53	0.07
165	-22.48	10.18	0.06
170	-21.76	7.86	0.06

Appendix B. Stable isotope ^{13}C and geochemical data from the isolation basin sediments.

Appendix C: Sediment core ITRAX XRF data access

This dataset can be reached at: https://docs.google.com/spreadsheets/d/1I2QCODUFvo-xWnMymMSRIKb0wSIGuauD4N6Wc_nd-yE/edit?usp=sharing